International Journal of Geo-Information

MDPI

Article

Frequent Fires, No Large Fires: A Landscape-Scale Assessment of Wildfire Risk Conditions and Response Capacity—A Case Study from South Korea

Miyeon An [1], Yunwon Choi [2] and Dongwoo Kim [3,*]

[1] Department of Landscape Architecture, Gyeongsang National University, Jinju 52828, Republic of Korea; myahn@gnu.ac.kr
[2] Department of Landscape Architecture, Pusan National University, Miryang 50463, Republic of Korea; yunwon.choi@pusan.ac.kr
[3] Climate, Environment and Energy Division, Gyeonggi Research Institute, Suwon 16207, Republic of Korea
* Correspondence: dwkim@gri.re.kr

Abstract

Wildfire risk arises from hazard, exposure, and vulnerability, but few studies ask whether the capacity to detect, suppress, and evacuate reaches places of high risk. Gyeonggi, South Korea, recorded 1272 wildfires in 2016–2026, yet none exceeded 100 ha. The purpose of this study is to map risk conditions and spatial proxies of response capacity on a 100 m grid and identify their mismatch. Risk conditions combined an ignition model, a Korea-adapted wildland–urban interface (WUI) rule, and evacuation-related vulnerability; response capacity combined camera viewsheds, fire-station distance, shelter travel times, and capacity. WUI residents (490,984) were older than average. Public shelter data recorded no wildfire designation, 99.9% of civil-defense shelters were underground, and listed above-ground capacity equaled 18% of WUI residents. In 28 municipalities with complete road data, 242,934 people lived in the top 20% of WUI risk cells; 23.8% were outside camera viewsheds and 9.9% over 30 min from a shelter at 20 km/h. Deficit locations were largely robust to analytical choices; deficit size varied with grid size and road speed, and municipal classes were unstable. Fire-station distance agreed only weakly with suppression records. A record without large fires does not imply low residual risk; the mapped deficits need field verification.

Keywords: wildland–urban interface (WUI); hazard–exposure–vulnerability; evacuation shelters; viewshed analysis; spatial mismatch

Check for updates

Academic Editors: Wolfgang Kainz and Godwin Yeboah

Received: 16 September 2026
Revised: 5 November 2026
Accepted: 7 November 2026
Published: 17 November 2026

Copyright: © 2026 by the authors. Published by MDPI on behalf of the International Society for Photogrammetry and Remote Sensing. Licensee MDPI, Basel, Switzerland. This article is an open access article distributed under the terms and conditions of the Creative Commons Attribution (CC BY) license.

1. Introduction

Global burned area is declining, but more people are exposed to wildfire. Although global fire activity decreased in 2001–2020, fires in the wildland–urban interface (WUI) increased by 23% in number and 35% in area [1], and in Catalonia, human exposure per unit burned area rose by 42–138% in 1992–2021 [2]. The global WUI grew by 35.6% after 2000 [3], a 10 m resolution map shows that it already covers large parts of the land surface [4], and in the United States, about half of the increase in houses within wildfire perimeters since the 1990s is explained by housing growth rather than by burned area [5]. The potential for loss thus depends increasingly on where people live, not only on how large fires become. Yet research on WUI and urban fires remains small relative to their share of global fire occurrence, and disciplines define and assess wildfire risk in different ways [6,7].

The IPCC describes climate-related risk as arising from the interaction of hazard, exposure, and vulnerability and recognizes that societal responses can change these components and the resulting risk [8]. A spatial assessment of wildfire risk must therefore consider where fires are likely to start and spread, who and what is located there, and how vulnerable they are. Outcomes also depend on whether a fire can be detected early, whether suppression resources can reach it and whether residents can move to a safe place. The IPCC treats such capacity as adaptive capacity within vulnerability [8], and index-based implementations such as INFORM fold lack of coping capacity into the risk score [9,10]; in disaster risk reduction terminology, the risk that remains after such measures is residual risk [11]. Integrated scores are useful for comparing overall risk but do not show directly which response is lacking where risk conditions are high. We therefore map risk conditions and response capacity as separate spatial axes and examine where they diverge.

Wildfire risk assessment systems emphasize different processes depending on their purpose. In the United States, large-fire simulation estimates burn probability and fire intensity for the risk assessment of mapped resources and assets [12]. The Canadian Forest Fire Danger Rating System combines daily fire weather with fuel-specific predictions of fire occurrence and behavior [13]. In southern Europe, ignition danger, propagation, and vulnerability have been integrated into GIS frameworks [14] and later reconciled in a pan-European wildfire risk assessment [15]. Russian forest fire protection relies on satellite and aerial detection combined with fire danger forecasts [16], and deterministic–probabilistic models have been developed for lightning-caused ignition in remote forests [17]. Australia introduced a national fire danger rating system with fuel-specific fire behavior models in 2022 [18]. These systems serve different purposes—daily forecasting, strategic risk mapping, or detection—and weight processes differently: lightning, for example, is central in boreal and remote forests but plays no role in a densely settled region where nearly all fires are human-caused. The present study does not replace such assessments; it maps risk conditions and compares, side by side, how far detection, suppression, and evacuation resources reach them.

Gyeonggi Province, South Korea, is a suitable case for this question. The metropolitan province surrounding Seoul is home to 14.12 million people, is 46.3% forested, and recorded 1272 wildfires between January 2016 and February 2026, the highest number in the country. Spatial clusters of high population density and high fire frequency are concentrated on the outskirts of the capital region [19], and among landscape, access, and settlement variables, distance to the forest edge has the strongest association with ignition in the province [20]. Yet the median burned area was 0.09 ha and 92% of fires burned less than 1 ha; the largest burned 29 ha, so none reached 100 ha, the area criterion for a large wildfire in Korea [21] (Figure S1).

Several explanations are possible for fires that are frequent but small, among them consistently successful initial attack and forest composition or weather conditions that limit spread; we do not separate them. Small past fires, however, do not show that the spatial conditions for resident evacuation are adequate. Public shelter data carry no wildfire designation, and the largest designated inventory with recorded capacity, the civil-defense shelters, is almost entirely underground (Section 4.5), so the location and capacity of above-ground destinations usable in a wildfire cannot be read from it. Because the protective actions available in a wildfire are evacuation away from the fire front and sheltering in place in a defensible above-ground structure or open space [22], the suitability of facilities for this hazard has to be established separately. Provincial wildfire planning, too, centers on the forest itself: the 2025 spring wildfire prevention plan of the provincial forest research institute, whose remit is the management of provincial forests, focuses on monitoring and initial attack [23].

The March 2025 wildfires in southeastern Korea (hereafter the 2025 Gyeongbuk wildfires) showed why resident evacuation matters when fires spread fast. The Uiseong fire reached an estimated peak spread rate of 8.2 km/h and on 25 March advanced about 51 km in roughly 12 h [24]. The fires in Gyeongbuk, Gyeongnam and Ulsan killed 30 people and damaged about 104,000 ha of forest and 3848 houses [25,26]. Most civilian victims were older adults, among them bedridden nursing-home residents [27]; evacuation orders were issued in the evening [28], and three nursing-home residents died when their evacuation vehicle was engulfed by fire at night [29]. Isolated villages of older adults and aging wooden houses jointly increased exposure and evacuation difficulty [30]. The case shows that spread rates must be considered together with the ability of residents to evacuate, the timing of evacuation and the means of transport.

The Ministry of the Interior and Safety (MOIS) subsequently revised the national evacuation system. Its 2025 guidelines call for immediate evacuation of zones that the predicted fire front reaches within 5 h, advance evacuation of vulnerable groups within 8 h, and evacuation of nursing homes before sunset when nighttime spread is expected [31]; follow-up measures included updating the standard wildfire manual and surveying forest-adjacent care facilities [32]. A January 2026 draft guideline calls for special care facilities within 100 m (Zone I) or 300 m (Zone II) of a forest boundary, or in isolation-prone areas, to identify at least two evacuation sites in advance [33]. Applying these standards in local plans requires knowing not only where forest-adjacent residents and facilities are, but also how long it takes to reach usable destinations and how detection and suppression resources are distributed.

Previous studies have addressed parts of this question. Wildfire risk indices usually focus on hazard and susceptibility, and when they include response capacity, it is limited to suppression resources and folded into the overall score; a modular index for Swedish rescue services and its multi-hazard extension are rare exceptions [34,35]. Korean studies have addressed nationwide ignition susceptibility [36], single-city cases [37], and ignition factors in Gyeonggi [20], and procedures for adapting WUI thresholds to local land use and settlement [38,39] have rarely been linked to wildfire risk and evacuation assessment in Korea. Evacuation research has examined evacuation decisions and departure times [40–43], coupled fire spread with walking and traffic [44], trigger boundaries for evacuation decisions [45,46], and social vulnerability [47] and road networks with few exits [48,49], but typically for one or two communities or a single fire, and regional risk maps have rarely been combined with travel times to shelters [50]. What is missing is a regional assessment that maps risk conditions together with spatial proxies of detection, suppression, and evacuation and identifies where high-risk conditions coincide with low response capacity.

The purpose of the study is to identify where wildfire risk conditions and the response capacity available to residents diverge in Gyeonggi Province, the metropolitan province surrounding Seoul, which serves as a case of frequent but small human-caused fires in a densely settled forest–urban landscape. The assessment is landscape-scale in the sense that it covers the whole forest–urban mosaic of the province—31 municipalities and about 10,390 km^2—rather than individual communities or fires, while results are computed and reported on a 100 m grid and used as a regional screening tool. Four objectives follow from this purpose, each addressed by a separate part of the analysis:

1. to map risk conditions—hazard, exposure and evacuation-related vulnerability—on a 100 m grid across the 31 municipalities (Sections 3.2–3.4, 3.7 and 4.1–4.3);

2. to represent detection, suppression and evacuation capacity by spatial proxies—camera viewsheds, fire-station distance, travel time to shelters and listed capacity—and to audit the designation, type, suitability and listed capacity of evacuation facilities (Sections 3.5, 3.6, 4.4 and 4.5);

3. to locate the cells and municipalities in which high-risk conditions coincide with low response capacity (Sections 3.1 and 4.6);

4. to test how far these results change with WUI thresholds, aggregation rules, index weights, travel speeds and grid size (Sections 3.8 and 4.7).

Keeping risk conditions and response capacity as separate axes, the study shows where the two diverge. It also adapts the WUI delineation to Korean settlement and forest landscapes, showing that the interface distance and the vegetation-share threshold, not the density threshold, govern the exposed population, and it links the hazard-specific limitations of shelter inventories and travel times to the location of high-risk conditions. The study does not propose a new risk index, nor does it measure detection times, suppression outcomes, or evacuation success in actual fires; instead, it screens at regional scale the areas that field surveys and evacuation planning should examine first.

2. Study Area and Data

2.1. Study Area

The study area comprises the 31 cities and counties (*si* and *gun*; hereafter municipalities) of Gyeonggi Province. Covering about 10,390 km^2, 46.3% forested (natural and planted forest in the Urban Ecological Status Map) and home to about 14.12 million people, the province surrounds Seoul in the central-western Korean Peninsula. Concentration in the capital region has strongly urbanized the areas around Seoul, especially southern Gyeonggi, so municipal population density ranges about 220-fold, from 66 persons/km^2 in Yeoncheon, the lowest, to 14,819 persons/km^2 in Bucheon, the highest. WUI population does not follow this gradient. Bucheon, the most urbanized municipality, has the smallest WUI population (675), whereas the largest (85,868) is in Gwangju, a city of relatively low density (955 persons/km^2; not to be confused with Gwangju Metropolitan City). Because urbanization and forest-adjacent population are distributed so differently, urbanization is treated as a potential confounder of the relationship between capacity and risk (Section 3.8); municipal values of all indicators are given in Table S1. The distribution of forest and WUI is shown in Figure 1.

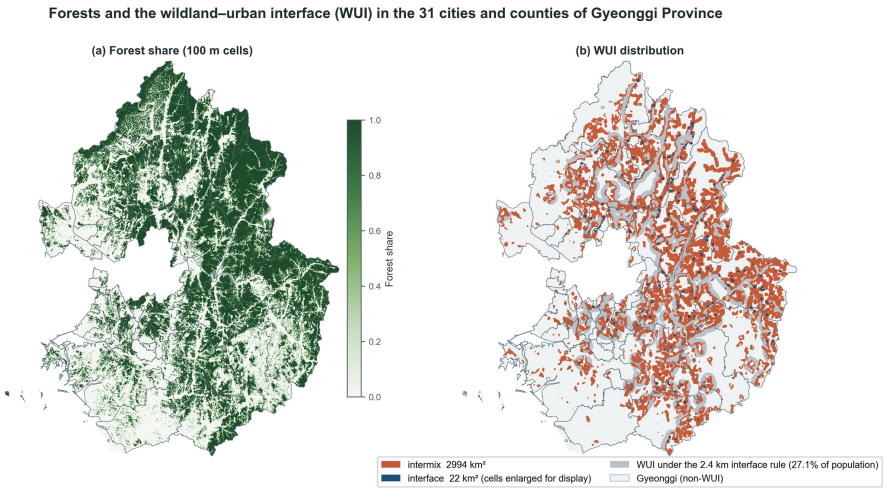


Figure 1. Forest share (**a**) and WUI distribution (**b**) in the 31 municipalities of Gyeonggi Province. The blank area in the center is Seoul. Intermix 2994 km^2, interface 22 km^2; WUI population 490,984 (3.5% of the provincial population). Gray in (**b**) marks the additional area classified as WUI under the original 2.4 km interface distance (27.1% of the population; Section 4.2), which extends into the dense urban areas around Seoul.

2.2. Grid System

Two grids are used together. A 20 m analysis grid (EPSG:5186, 7704 × 6504 cells) carries land cover, distances, terrain, and fuel; it is rasterized at 10 m and max-pooled 2 × 2 so that narrow roads are not lost. A 100 m master grid (EPSG:5179, 1542 × 1305 cells, of which 1,037,839 lie in Gyeonggi) carries population, households, housing and older adults, and is the grid on which the indices are composed and all final outputs are produced.

The two grids are separated because the data differ in nature. Population grids are count data whose values are distorted by reprojection, so they are kept in their original coordinate system, and forest, terrain, and hazard layers are transferred to that grid. Distance and slope calculations, conversely, require 20 m resolution. Each 100 m cell was assigned to the municipality given by the mode of the 20 m municipal codes.

2.3. Data

The datasets, their sizes, and their reference periods are listed in Table 1.

Table 1. Data sources and reference periods.

Category	Dataset	Size	Reference Period
Wildfire	Wildfire register	1272 fires (ignition date and time, time of main-fire containment, cause, burned area)	Jan 2016–Feb 2026
Wildfire	Ignition parcels	Retrieved for 1250 fires; 1176 on burnable land used for modeling	Jan 2016–Feb 2026
Fuel	Urban Ecological Status Map (biotope map), final GDB	1,871,863 polygons	2026
Fuel	Forest type map of the Korea Forest Service (FRTP and KOFTR layers)	180,244/275,955 polygons	5th edition
Terrain	Elevation, slope and aspect from the national 90 m digital elevation model (DEM)	20 m raster (resampled from 90 m)	—
Population	100 m grid of population, households and housing from the Statistical Geographic Information Service (SGIS)	1,041,938 cells	2024
Population	National Land Statistics 100 m grid of older adults (aged 65 or older)	2,474,823 persons (17.5%)	Oct 2024
Vulnerable facilities	Elderly, education, hospital, disability, mental health and special-school lists published on the Gyeonggi Data Dream open data portal	35,315 (after removing cross-file duplicates)	2026
Vulnerable facilities	Residents of elderly medical-welfare facilities	2140 facilities, 72,908 residents	2026
Response	Equipment inventory (17 spreadsheet tables)	Cameras 250 installed and 2 planned (237 analyzed), lookout towers 68, guard posts 169, suppression vehicles 143 and other equipment	Feb 2026
Response	Fire stations/heliports/wildfire response centers	35/19/12	2026

Table 1. *Cont.*

Category	Dataset	Size	Reference Period
Evacuation	Civil-defense shelters (in use, Gyeonggi)	4052	Mar 2026
Evacuation	Landslide-vulnerable-area shelters	994	Mar 2026
Roads	Road centerlines, continuous digital topographic map	1,985,065 LineStrings	2026
Cadastre	Continuous cadastral map	5,210,398 parcels	May 2026

The register attributes every fire to a human or unknown cause: of its 13 cause categories, the largest are hikers (248 fires), unknown (220), refuse burning (211) and cigarettes (134), and none of the 1272 fires is attributed to lightning. Hydrography is not among the inputs. The ignition covariates follow the final specification of the preceding study of the same register [20], in which distances to settlements, farmland, trails and forest edges represent the human activities through which fires start. Streams and rivers here run mainly through corridors of settlement and farming, whose effects these distances already capture, and no cause category refers to them.

Fuel areas by forest class come from the forest type map, which delineates forest slightly differently from the biotope map used in Section 2.1; each source is used only within the layer it defines (Text S1).

After removing records outside the province and duplicates between and within files (Text S1), 35,315 facilities were used. All lists come from the provincial open data portal, so facilities it does not publish are absent, and the counts are lower bounds.

People unable to evacuate on their own were defined as the 72,908 residents (2140 facilities) of elderly medical-welfare facilities under Article 34 of the Welfare of Senior Citizens Act [51]. Elderly residential-welfare facilities, which house older adults capable of daily living and lie outside the national guideline for wildfire-vulnerable special care facilities (hereafter the care-facility guideline) [33], were assigned to the assisted-evacuation tier, and their residents were not counted (Section 3.4; Text S1).

2.4. Data Processing Conventions, Identified Defects and Their Effects

The source data contain several defects. Their expected effects on the results are summarized here; quantified effects are reported in Section 4, and record-level details in Text S1.

The population and older-adult grids suppress small counts to zero. Suppressed zeros were replaced with 2, a mid-range value for suppressed small counts, and nulls with 0. The two grids also differ in source and date (the 2024 SGIS grid and the October 2024 National Land Statistics grid), and in 13,830 cells the number of older adults exceeds the total population. Because shares are computed from window or regional sums (Sections 3.4 and 4.3), this mismatch does not produce shares above one. The replacement value matters more: it moves the older-adult share of the WUI population between 18.0% and 28.2%, so only the direction of the difference from the province is robust (Section 4.3).

Ignition coordinates in the register are parcel centroids. A previous study showed that they are displaced toward roads and buildings—81.3% of records denote forest lots, but only 37.5% of coordinates fall on forest lots [20]—and in the register up to 17 records on different dates share the same coordinates. A case–control probability surface built from random points within the ignition parcels was therefore used (Section 3.2). Its values are relative ranks, which suffice for the percentile-based index but not for statements about expected numbers of fires. The register ends in February 2026 (Figure S1), which affects fire counts but not the location model.

The housing grid has no housing type, so the residential classes of the biotope map were used instead. Because most cells have almost no residential land and were imputed (Section 3.4), this component adds little information and changes V little (Section 4.7).

Of the 250 installed cameras, 13 recorded as broken, aging, or awaiting repair were excluded, leaving 237 cameras at 152 sites; these status decisions move camera coverage of the WUI population between 63.4% and 66.4% (Section 4.7). Lookout towers and guard posts have no coordinates, so their coverage can be estimated only as an upper bound (Section 3.5), and camera-based detection deficits describe automated monitoring rather than all monitoring.

The facility lists come from the provincial open data portal and do not include residents of residential disability facilities, so vulnerability is understated rather than overstated. Land cover (2026) and households (2024) postdate many of the fires, which matters most in recently developed areas. Finally, road centerlines are withheld near the inter-Korean border: road cells cover 7.9%, 13.4% and 27.4% of all cells in Yeoncheon, Paju and Gimpo, against a municipal median of 63.9%. Travel-time results are therefore reported for the other 28 municipalities, with province-wide values for reference (Section 3.6).

In sum, the defects affect the magnitude of individual estimates—the older-adult share, detection coverage and travel times in three border municipalities—but not the inventory-based findings on shelter designation, type and listed capacity, which rest on counts that none of these defects alters.

3. Methods

3.1. Conceptual Framework—Risk Conditions and Response Capacity

The first axis is that of risk conditions. Following the IPCC AR5 risk framework [8], the spatially existing risk condition is represented as $R = (H \cdot E \cdot V)^{(1/3)}$ (Section 3.7), where H is wildfire hazard (ignition probability × spread potential, Section 3.2), E is the exposed population living in the wildland–urban interface (Section 3.3), and V is evacuation-related vulnerability (Section 3.4). R describes where a fire is likely to start and spread, who lives there and how able they are to evacuate on their own; it says nothing about what would happen once a fire starts.

Terms for wildfire risk differ among disciplines [7]. In fire management, fire danger usually denotes the likelihood that a fire starts and spreads, as determined by fuels, terrain and weather, and risk denotes that likelihood combined with the expected loss of ecological, economic or social values [12,14]. Under the IPCC definition adopted here, risk is the potential for adverse consequences that arises from hazard, exposure and vulnerability, and it does not require losses to be valued [8]. In this sense, H corresponds to a static, long-term fire danger, and R adds who lives where a fire may start and spread and how able they are to evacuate. R does not estimate expected damage to people, property or ecosystems. We therefore call R the risk conditions, H the hazard, and reserve fire danger for the established rating systems that forecast daily danger from weather and fuels [13,18].

The second axis is the management or adaptive capacity that can reduce that risk [8]: C for detection and suppressive response (viewsheds of wildfire cameras and distance to fire stations, Section 3.5) and EC for evacuation response (travel time to above-ground shelters, listed shelter capacity and detection, Section 3.6). Both are computed for the resident's cell, so they express the capacity available to the people who live in a given risk condition rather than the capacity of the response system as a whole. They are spatial proxies built from the location of response assets, not observations of response performance such as detection or arrival times; Section 3.5 describes a partial check of the suppression component against the suppression records of the register, whereas the detection component cannot be validated with the available records.

Response capacity is not treated as a fourth component of the risk index, because the purpose of this study is to diagnose the spatial mismatch between the underlying risk conditions and the capacity available to reduce them. Folding capacity into the index, as INFORM does with lack of coping capacity [9,10], is useful for ranking but hides exactly that mismatch; an INFORM-type form, $(H{\cdot}E{\cdot}V{\cdot}(1-C))^{(1/4)}$, is therefore reported only as a sensitivity analysis (Section 4.7). Reporting exposure and social vulnerability separately follows previous practice [52,53]. In disaster risk reduction terminology, the risk that remains after capacity is taken into account is residual risk [11]; the mismatch analyzed here is a spatial approximation of it, not a quantification.

The two axes are combined in two ways. Cells in the top-20% risk class (Section 3.7) are crossed with the response deficits measurable at cell level—travel time to a shelter beyond 30 min and location outside camera viewsheds—and municipalities are placed in quadrants by the median of R and the median of each capacity (Section 4.6). The overall workflow is shown in Figure 2.

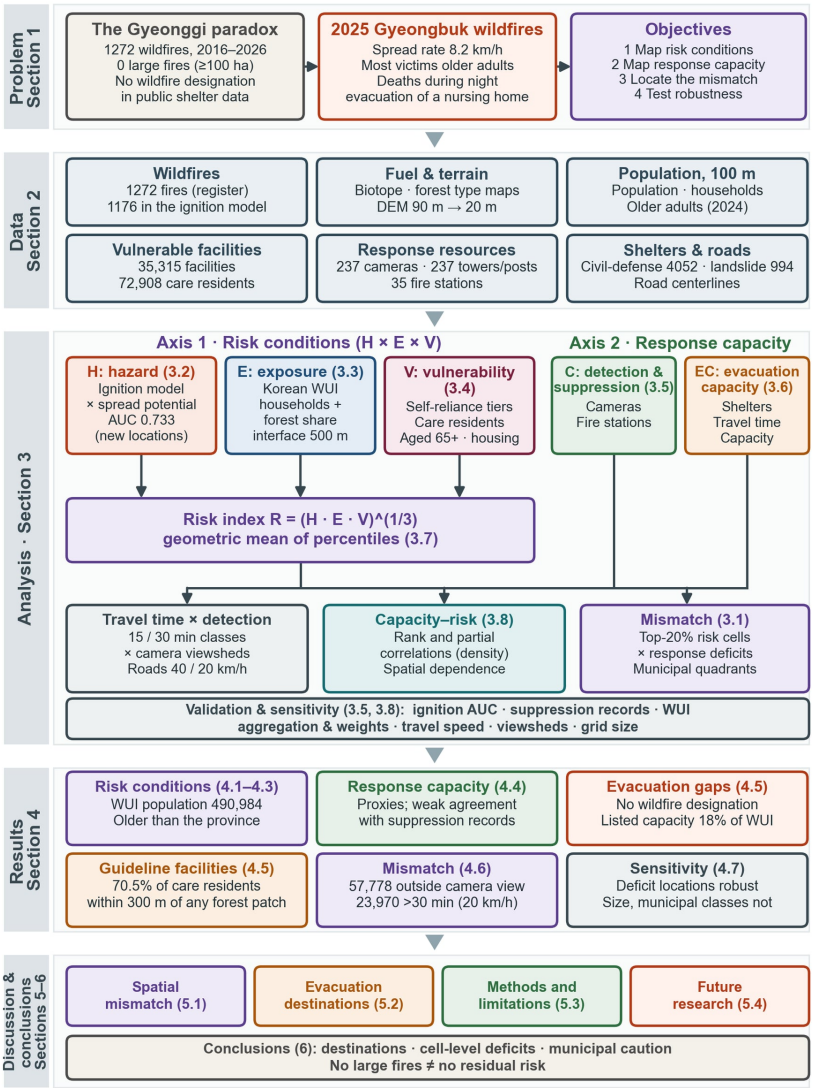


Figure 2. Research workflow—from problem definition and data, through analysis along two axes (risk conditions R; response capacity C and EC), to results and discussion. Numbers in parentheses refer to manuscript sections.

3.2. Hazard H = Ignition Probability × Spread Potential

3.2.1. Ignition Probability Surface

Past ignition points serve here as training labels, not as a hazard layer. Using ignition density as hazard implies the circular reasoning that fires will recur because they occurred before, and our parcel-centroid points make that density unreliable. We therefore fitted a case–control logistic regression (random points within ignition parcels versus random background points) and applied its coefficients to province-wide covariate rasters. The model design follows the final specification of a previous study of the same register [20]. That study also showed that associations with hiking trails differ by ignition cause [20]; a single model is used here because the hazard surface is meant to cover all human-caused fires, and cause-specific models would shrink each sample without changing the response-capacity analysis. Road distance was not included as a separate covariate. In this densely roaded landscape, 85.0% of the forest lies within 500 m of a road at least 3 m wide, and in that study, road distance, although it differed between ignitions and controls, added little independent information beyond forest-edge distance and settlement (odds ratio 0.969); an association appeared when ignitions were assumed to lie near access routes [20]. Road access is therefore represented largely through the forest-edge and settlement covariates; this does not imply that roads are unrelated to ignition. Road centerlines are also withheld in parts of Yeoncheon, Paju, and Gimpo, so omitting the term allowed all 31 municipalities to be covered. To use the model as a hazard surface, we added temporal and novel-location validation, as in the family of procedures used to derive 100 m human-caused ignition probability surfaces for five European pilot sites [54]. Because of the case–control design, surface values are relative ranks rather than absolute ignition probabilities. As the preceding study notes, the model describes which landscape conditions are associated with ignition rather than predicting individual ignitions [20]; the surface is used here only as a relative ranking within the index.

Each fire was represented by N random points within its ignition parcel, $N = \min(\max(\lceil \text{parcel area in ha} \rceil, 5), 40)$, each weighted 1/N so that every fire has a total weight of one; larger parcels, where the ignition location is more uncertain, thus receive more points but not more weight. Background points were drawn at random from burnable land within the province. Eleven covariates were used: distances (log-transformed) to hiking trails, settlements, farmland and forest edges; edge density and forest share within a 500 m disk; household density (log-transformed); elevation; slope; northness; and eastness. The model was fitted to 11,316 points within the parcels of 1176 fires against 18,398 background points (about 1:15.6 by fire). Coefficients of the 31-municipality fit and of a 28-municipality fit that omits the three border municipalities, as the preceding study did [20], are given in Table S2. Every covariate except eastness (odds ratio 0.985, $p = 0.62$) is significant at the 5% level, and the two fits agree in direction and size.

Validation was twofold: a temporal split (training on 2016–2022, predicting 2023–2026) and a novel-location test restricted to validation fires more than 500 m or 1 km from training-period fires (Section 4.1). Lightning is not represented, because no fire in the register was attributed to it (Section 2.3), so the model describes human-caused ignition. Where cloud-to-ground lightning is a major ignition source, lightning density or thunderstorm-based danger criteria would be needed as additional hazard components [17].

3.2.2. Spread Potential

Ignition probability alone does not identify where fires grow large. Following a Korean study showing that conifer share and mature forest drive burned area [55], we combined fuel and terrain components into a spread-potential index (Equation (1)):

$$SP = F \times (0.4 \cdot P + 0.4 \cdot S + 0.2 \cdot Q) \quad (1)$$

Here F is a fuel score (*Pinus* 1.0, other conifers 0.85, mixed 0.7, broadleaf 0.4, non-stocked forest 0.2, non-forest burnable land 0.15 and non-burnable land 0); P is forest continuity, $\min(\max(\log_{10} a/2, 0), 1)$ for the area a (ha) of the 8-connected forest patch, which reaches 1 for patches of 100 ha or more; S is slope, $\min(\text{slope}^\circ/35, 1)$; and Q is aspect, $(1 - \text{northness})/2$, which is 1 on south-facing slopes. Fuel scores and component weights reflect expert judgment and were not derived from experiments or fire-spread simulations. Their contribution was evaluated by discriminating fires of 0.5 ha and 1 ha or more from background (Section 4.1); because that gain was not statistically significant, the spread component is treated as an unvalidated, expert-based term, and the analysis was repeated with an ignition-only hazard (Section 4.7). Wind is not included because the map is static, whereas wind speed and direction vary from day to day and dominate spread during individual events, and no wind field at a resolution compatible with the 20 m grid was available; the map therefore complements rather than replaces daily fire danger forecasting (Section 5.3).

3.3. Exposure E—Korean WUI Mapping

We apply Radeloff-type rules [56,57] to focal windows rather than to individual cells (Table 2), because a single dwelling in a 100 m cell already implies a density of 100 dwellings/km^2, so cell-level density thresholds cannot discriminate.

Table 2. WUI classification rules.

Criterion	Value
Density	Household density in a 1 km window >6.17 households/km^2
Intermix	Density criterion met & forest share in the window ≥0.50
Interface	Density criterion met & forest share in the window <0.50 & within 500 m of a large vegetation patch (forest share ≥0.75 in a window of about 5 km^2)

Two adjustments were made. The first replaces housing units with households, because Korean statistics exclude non-dwelling residences such as vinyl greenhouses and containers from "housing", an undercount concentrated in forest-adjacent rural areas. The threshold of 6.17 households/km^2 carries over the 6.17 housing units/km^2 of the original rule [56]; this adjustment and the window-based density rule follow a previous study [20].

The second shortens the interface distance from 2.4 km, which derives from crown-fire spotting in the western United States, to 500 m. Applied to Gyeonggi, 2.4 km raises the WUI population eightfold, from 3.5% to 27.1%, with 57% of that population in apartment cells of more than 300 residents, which blurs the focus on forest-edge residents. In 23 fires in southern Europe, WUI damage severity also decreased as surrounding buildings became denser [58]. The largest fire recorded in Gyeonggi (29 ha, an equivalent radius of about 300 m) is a weak basis, because small past fires may reflect suppression capacity or landscape conditions.

More direct evidence comes from the 2025 Gyeongbuk wildfire. Of 1669 houses damaged outside the burned forest, the median distance to forest was 67.3 m and 95.0% lay within 300 m; on this basis, the national guideline extended the scope for special care facilities to 300 m from a forest boundary (Zone II) [33]. Field checks had removed duplicate or erroneous addresses and locations beyond 500 m, so the distribution shows

where most damage occurred, not whether it extended farther. We therefore use 500 m and also report 1 km and the original 2.4 km rule (Sections 4.2 and 4.7). Because this WUI relies on forest share in a 1 km window and on large vegetation patches, it excludes urban residents next to small forest patches, so WUI-based evacuation gaps are conservative (Sections 4.5.5 and 5.3).

3.4. Vulnerability V—Evacuation Self-Reliance

Vulnerable facilities are weighted by evacuation self-reliance rather than divided into day and night uses. First, 83.6% of wildfires in Gyeonggi start between 09:00 and 18:00, peaking at 13:00–14:00, and only 3.7% between 00:00 and 06:00, so senior community centers and daycare centers are occupied at ignition. Second, people present at the same time differ in their ability to evacuate: a bedridden nursing-home resident is not comparable to a visitor of a senior community center. This distinction is supported by reports that care facilities are the most vulnerable in terms of wildfire proximity [59], that older age and disability are core indicators of social vulnerability [52] and that social vulnerability affects evacuation rates, departure delays and distances [47], and by a planning model that triages vulnerable people by health status for early transport [60].

Facilities were therefore assigned to three tiers of evacuation self-reliance (Table 3).

Table 3. Three tiers of evacuation self-reliance (after de-duplication).

Tier	Weight	Facilities	Types
T1 Unable to self-evacuate	1.0	2481	Nursing homes and long-term care group homes (elderly medical-welfare facilities), long-term care hospitals, psychiatric hospitals
T2 Assisted evacuation	0.5	19,651	Residential homes, group homes and welfare housing for older adults (elderly residential-welfare facilities), general and emergency hospitals, daycare centers and kindergartens, special-education schools, disability-inclusive daycare
T3 Self-evacuating	0.2	13,183	Senior community centers, senior welfare centers, primary and secondary schools, clinics

Elderly residential-welfare facilities are placed in T2 because their residents need housing and meal services, whereas elderly medical-welfare facilities house older adults who need assistance because of substantial physical or mental impairment [51].

Facility counts are weighted rather than summed. Senior community centers and daycare and education facilities make up 90% of all facilities, so an unweighted sum would let facility density stand in for population density and count exposure twice (Spearman 0.753 between the two alternatives across Gyeonggi cells; Section 4.7).

Facility points are smoothed with a 500 m disk kernel, matching the near-forest exposure distance of the WUI interface. Counted per cell, only 2.4% of Gyeonggi cells would have a value, making V practically constant; the kernel extends coverage to 40% of cells.

$$V = 0.30 \cdot \mathrm{pct}(\text{weighted facility count}) + 0.20 \cdot \mathrm{pct}(\text{residents unable to self-evacuate}) + 0.35 \cdot \mathrm{pct}(\text{older-adult share}) + 0.15 \cdot \mathrm{pct}(\text{detached housing share}) \quad (2)$$

The weights of Equation (2) reflect expert judgment, with the largest weight on the older-adult share (alternatives in Section 4.7; pct() in Section 3.7). To avoid shares of 100% in suppressed cells, older adults and total population are summed separately within the 500 m window; windows with fewer than 50 people (42.7% of cells) take the provincial mean. The detached housing share comes from the medium classes of the biotope map. Detached and low-rise houses require individual defense and more often have wooden or aging structures [5,30], and distance to neighboring buildings and surrounding canopy

cover are associated with house loss [61]. Cells with less than 1% residential land (84.9%) take the WUI mean, because a provincial mean would be pulled down by urban apartment land. Evacuation facilities are a capacity and are treated in Section 3.6, not in V.

3.5. Suppression and Detection Capacity C

Detection is represented by line-of-sight viewsheds of the 237 operational cameras, computed on the DEM with a radial algorithm that walks outward along 720 azimuthal profiles. Observer heights are 25 m for lookout-type, 15 m for close-range, and 40 m for pylon-mounted cameras; the target is 10 m above the ground to represent a smoke column, and the maximum radii are 20, 5, and 15 km, respectively. The radii are assumptions, because the inventory records no daytime detection range, and Earth curvature and obstruction by trees and buildings are not modeled. The visibility of a residential cell is used as a proxy for whether fires in the surrounding forest can be seen, following studies that compared lookout-tower viewsheds with detection records [62] and optimized camera networks [63,64]. Lookout towers and guard posts, which have no coordinates, were located from their lot numbers and added as an upper-bound estimate (Text S1).

Suppression access is the straight-line distance to the nearest of 35 fire stations, used in the same way to plan wildfire access routes [65]. It ranks municipalities almost identically to road-weighted travel time from the same stations (Spearman +0.976 across the 31 municipalities and +0.994 across the 28 with complete road data; Table S3). Neighborhood 119 safety centers (119 being Korea's fire and rescue emergency number) and municipal wildfire crew bases could not be included because their locations are not available to us. Heliports and equipment were left out because helicopters are dispatched across the province and equipment counts are municipal totals without locations. C is therefore a coarse proxy for suppression access:

$$C = 0.5 \cdot \mathrm{pct}(\text{camera visibility}) + 0.5 \cdot [1 - \mathrm{pct}(\text{distance to fire station})] \quad (3)$$

The equal weights are an expert choice; alternatives are tested in Section 4.7.

Because C is a proxy, it was compared with operational records. For the 1249 fires whose retrieved ignition parcel lies on the 100 m grid (parcels were retrieved for 1250 fires, and one parcel lies outside the grid), the camera visibility and fire-station distance of the 100 m cell containing the parcel were related to the time from ignition to containment of the main fire and to the burned area, using Spearman correlations, comparisons of medians and log-linear regressions with year fixed effects; municipal C was related to the municipal median containment time and to the share of fires of 1 ha or more. The register does not record detection times, and only 3 of its fires were reported by a camera, whereas 1057 list the fire service as the reporting party, so the detection component cannot be checked in this way.

3.6. Evacuation Capacity EC

3.6.1. Terms and Audit of Evacuation Facilities

We first distinguish terms. An evacuation destination is any place evacuees head for. A designated shelter is a facility designated under statutes or guidelines (civil-defense shelters and landslide-vulnerable-area shelters, hereafter landslide shelters). A potential above-ground destination is a designated shelter that is above ground and could be used in a wildfire but has not been assessed for that purpose; the landslide shelters used here belong to this category. A wildfire-verified safe destination would be one assessed for separation from forest, construction, and suitability for staying; no such list exists in the public data. An outdoor refuge is an open space used temporarily when trapped by fire. Capacities in

this study are the maximum numbers listed in the shelter data (listed or nominal capacity), not capacities verified for wildfire use.

Evacuation destinations are defined in three ways (Table 4), and travel time is computed for each.

Table 4. Definitions of evacuation destinations.

Definition	Facilities Included	Sites (Origin Cells)	Capacity (Persons)
strict	Landslide shelters in use and able to host temporary stays	491 (488)	40,615
base	Landslide shelters in use	979 (945)	86,987
civil-defense (designated inventory)	Civil-defense shelters in use (4047 of them underground)	4052 (3771)	50.99 million

Origin cells are counts after merging facilities that fall in the same 100 m cell. Hereafter, strict shelters denote destinations under the strict definition. Because public shelter data contain no wildfire designation, landslide shelters (senior community centers, village halls, etc.) are used as proxies for above-ground evacuation destinations. That they have not been assessed for wildfire suitability is a limitation. The base definition is used for capacity comparisons, because any shelter in use adds places, and the strict definition is used for travel times, because evacuees may need to stay for hours. The open/closed field of the shelter data is not used: the 158 shelters in use but recorded as not open, concentrated in Gapyeong, Namyangju and Anseong, are village halls and senior community centers like the others, so the field appears to record whether a facility is routinely open rather than whether it is available.

3.6.2. Travel Time on a Road-Weighted Grid

On an 8-neighbor grid graph (1,037,839 nodes, 8,269,842 edges), with 11.1 m/s (40 km/h) on road cells and 1.1 m/s (walking at 4 km/h) elsewhere, all shelters serve as simultaneous sources of the shortest travel time. Roads are the centerlines of the continuous digital topographic map used in a previous ignition study [20]; a 100 m cell is a road cell if it contains any 20 m road pixel. Because centerlines are withheld in parts of Yeoncheon, Paju, and Gimpo (Section 2.4), results are reported for the other 28 municipalities, with province-wide values for reference. Because 40 km/h is optimistic in smoke, at night, in congestion, or on narrow farm roads, the calculation is repeated at 5.6 m/s (20 km/h), and results are given as a range. An off-road walking speed of 0.79 m/s, 72% of that of the general population as reported for older adults [31], was also tested.

The approach resembles a study in central Portugal that combined shelter travel time with hazard and social vulnerability to prioritize evacuation areas [50]. Unlike agent-based models of congestion and departure delay [44,66], it computes only the shortest time per cell. Absolute times are therefore lower bounds that exclude warning reception, preparation, and departure delays, suited to regional comparison. Shelters and roads outside Gyeonggi are excluded. Results are reported by descriptive travel-time classes (15 and 30 min), not safety standards, crossed with camera viewsheds.

Shelter capacity does not constrain the shortest-time calculation. To show its effect, each WUI cell was assigned to its fastest-reached base shelter (shelters in the same 100 m cell merged), and the assigned population was divided by listed capacity. The population at overloaded shelters and the summed excess show how much of the shortfall arises from where capacity lies. This nearest-shelter load does not reassign people turned away, which would require a network-flow model with explicit behavioral rules (Section 5.4). It therefore measures capacity pressure and is not a capacity-constrained evacuation analysis.

3.6.3. Evacuation Capacity Index and Guideline-Scope Facilities

$$EC = 0.40 \cdot [1 - \text{pct}(\text{travel time})] + 0.35 \cdot \text{pct}(\text{camera visibility}) + 0.25 \cdot \text{pct}(\text{municipal capacity ratio}) \quad (4)$$

Detection is included in EC because it advances the start of evacuation. Equation (4) is an expert-weighted composite, not a model fitted to experimental data or simulation results: the largest weight is placed on travel time, which the analysis measures most directly, and the smallest on the capacity ratio, which is a municipal quantity. Three alternative weightings and a version without camera visibility are tested in Section 4.7, and EC is used only for comparisons among municipalities. Camera viewsheds enter both C and EC, so part of the correlation between the two capacities comes from this shared component. The municipal capacity ratio is the base-definition capacity of a municipality's landslide shelters divided by its WUI population; it counts only the municipality's own shelters and does not reflect the use of shelters in neighboring municipalities.

Facilities within the scope of the national guideline were counted separately. Following the scope of the *Guideline for Evacuation Planning at Wildfire-Vulnerable Special Care Facilities (Draft)* [33], distances from elderly medical-welfare facilities and hospital-level medical institutions (excluding clinics; records sharing coordinates counted once) to the 20 m natural and planted forest grid of the biotope map were measured, and facilities were classified into Zone I (within 100 m of a forest boundary) and Zone II (within 300 m, which contains Zone I). The travel times to strict shelters (roads at 40 and 20 km/h) and camera and tower visibility of the 100 m cell containing each facility were attached. Isolation-prone areas (surrounded by forest or with a single access road) were not evaluated because data for identifying access roads were unavailable.

3.7. Risk Index R

$$R = (H \cdot E \cdot V)^{(1/3)} \quad (5)$$

All components are converted to percentiles, because their native units differ by orders of magnitude. The function pct(x) is the percentile rank of a cell's value among all 1,037,839 cells of Gyeonggi, with ties receiving the average rank (reference sets and rules in Table S4). For components that are zero where the quantity is absent (hazard on non-burnable land, population in unpopulated cells, facility counts), zeros stay zero, and only positive values are ranked to $(0, 1]$, so that zeros do not inflate the ranks of small positive values. Distances and travel times are inverted as $1 - \text{pct}()$, so that higher values always mean greater capacity.

Equation (5) is the geometric mean, $R = \exp[(\ln pH + \ln pE + \ln pV)/3]$, a form common in index-based implementations of the IPCC risk framework [9] and usual when compensation among components should be limited [67]. Its elasticity with respect to each component is 1/3, so a 10% lower value of any component lowers R by about 3.5%, whereas under the arithmetic mean a high component can offset a low or zero one. R is zero if any component is zero: there is no risk without hazard or without people. Because the geometric mean is dominated by its smallest component and E is low in most WUI cells, R is sensitive to exposure (Section 4.7).

R is an intensity index: the risk borne by an individual WUI cell, not the total borne by a municipality. Because E is a population percentile across all Gyeonggi cells, urban municipalities with densely populated WUI cells obtain high R (Bucheon 0.811 with a WUI population of 675), so totals are reported separately as WUI population and population in top-20% risk cells. R is thus associated with population density by construction, and H contains household density and distance to settlements; this is considered in the capacity–risk comparisons (Section 4.4). Because E is zero outside the WUI, $R > 0$ only inside it.

Cells at or above the 80th percentile of R among WUI cells with $R > 0$ ($R \geq 0.62$) form the top-20% risk class (Sections 3.1 and 4.3–4.6).

3.8. Sensitivity Analysis

The subjectivity of weights is a recurrent weakness of wildfire risk indices; a review of 112 studies from 2015–2025 found that multi-criteria decision analysis accounts for 44% of approaches and that preferred indicators differ among regions [68]. We therefore varied the analysis in seven groups, specified in full in Text S1: WUI thresholds, changed one at a time [38]; the risk index, through reweighting, the arithmetic mean, an INFORM-type four-component form and an ignition-only hazard; the components and weights of V; the weights of C and EC, including EC without camera visibility; road and walking speeds, camera sets, the shelter open/closed field and observer height; the provincial edge; and the grid, by re-aggregating the cell-level results to blocks of 200 m, 500 m and 1 km. Because the arithmetic mean is positive whenever any component is positive, it was evaluated both over all WUI cells and over the cells on which the baseline is defined. Each alternative was judged not only by the rank correlation of municipalities but by what it changes for the places and people the study identifies: the overlap of the top-20% risk cells, their population and response deficits, and the membership of the high-risk·low-response quadrants across all combinations of risk and capacity indices.

The relationships between capacity, risk and urbanization were examined as simple and partial Spearman correlations controlling for WUI population or municipal population density (rank-residual method), together with the converse partial correlations of density with capacity given R. Because municipal values are spatially autocorrelated, effective sample sizes were estimated following Clifford et al. [69] and Dutilleul et al. [70], the partial correlations were repeated with the spatial lag of capacity as a control, and all indices were also aggregated in the same way, since municipal R is population-weighted whereas C and EC are means over WUI cells. With 31 spatially dependent units and no correction for multiple comparisons, these relationships are treated as descriptive associations; bootstrap intervals (5000 resamples) are reported to show their width rather than to establish significance.

3.9. Reproducibility

The analysis scripts, their run times, and their main outputs are listed in Table S5; the pipeline and the order in which the scripts are run are documented with the deposited code.

All analyses were carried out in Python 3.12 with NumPy 1.26, pandas 3.0, GeoPandas 0.14, Shapely 2.0, Rasterio 1.4, pyproj 3.6, SciPy 1.17, statsmodels 0.14, scikit-learn 1.8 and Matplotlib 3.8. QGIS Desktop 3.30.1 (QGIS Development Team, Open Source Geospatial Foundation) was used only to inspect input data and intermediate outputs visually; all analytical steps, including rasterization, focal statistics, the radial line-of-sight viewshed, and the grid travel-time graph (multi-source Dijkstra in scipy.sparse.csgraph), were implemented as scripts. The analyses were run on a laptop with an Intel Core i9-13900H processor (14 cores) and 16 GB of memory under Windows 11. Every script documents data sources, processing steps, and output paths in its header. Random seeds are fixed, and intermediate outputs are saved with versioned file names.

4. Results

4.1. The Ignition Surface Generalizes to New Locations

The area under the receiver operating characteristic curve (ROC-AUC) of the temporal validation was 0.736 (bootstrap 95% CI 0.713–0.759, from 2000 resamples drawing validation

fires and background points independently; Table S3). This lies within the 0.70–0.89 range reported for 100 m human-caused ignition models at five European pilot sites [54] and below the 0.829 of a nationwide Korean model that used nonlinear models and a national sample [36].

In the novel-location validation, cells more than 500 m from training-period fires gave an AUC of 0.733 (95% CI 0.704–0.763) and cells more than 1 km away 0.727 (0.692–0.764), with the same validation background points; both intervals overlap that of the temporal split. Adding the spread component raised the AUC for separating the ignition points of larger fires from background from 0.713 to 0.739 for fires of 1 ha or more (99 fires) and from 0.745 to 0.763 for fires of 0.5 ha or more (212 fires). Neither gain was statistically significant (two-sided DeLong test for correlated ROC curves, $p = 0.066$ and 0.061; bootstrap 95% confidence intervals of the difference −0.002 to +0.054 and 0.000 to +0.038; Table S3).

4.2. The Interface Distance Governs the Size of the WUI

Under the adjusted rules, the WUI covers 3016 km^2 (intermix 2994 km^2, interface 22 km^2), with 490,984 residents (3.5% of the provincial population), 4.0% of households and 4.2% of housing units.

Widening the interface distance to 1 km increases the WUI population to 805,725 (5.7%) and lowers listed above-ground shelter capacity from 18% (Section 4.5) to about 11% of the WUI population; the municipal rank correlation is 0.933. Under the original Radeloff rule of 2.4 km, the WUI population rises eightfold to 27.1%, 57% of it in apartment cells with more than 300 residents each, and the municipal rank correlation falls to 0.750 (Figure 1b). Other threshold changes hardly affect rankings, although the vegetation-share threshold changes the size of the WUI population to 7.3% at 0.4 and 1.9% at 0.6 (Section 4.7).

4.3. WUI Residents Are Older, Live in Detached Housing and Concentrate in High-Risk Cells

The share of older adults among WUI residents is 23.1%, 5.6 percentage points above the provincial 17.5%. Replacing suppressed values with 1–3 persons gives 18.0–28.2% for the WUI and 16.8–18.3% for the province, and using only cells with at least five residents gives 21.0% versus 17.3%. The size of the difference (1.2–9.9 percentage points) is uncertain, but its direction holds. The share is highest in Yeoncheon (36.4%), Dongducheon (33.0%), Bucheon (32.3%), Yangpyeong (31.3%), and Gapyeong (30.8%).

Detached housing accounts for 94.6% of residential land in the WUI and 76.9% province-wide, from 100% in Osan and Yeoncheon to 22.8% in Bucheon (Text S1).

Of the 72,908 residents of elderly medical-welfare facilities, 9471 live in 254 facilities in WUI cells, and 10,971 within a 500 m zone of influence.

Hazard, driven mainly by spread potential, is highest along mountain ridges, exposure appears in settlements at mountain edges, and vulnerability occurs where facilities and older populations overlap (Figure S2).

The top-20% risk class ($R \geq 0.62$; Section 3.7) holds 249,231 people, 50.8% of the WUI population. Of this population, 41.7% live in Gwangju (18.6%), Seongnam (11.7%), and Yongin (11.4%) (Figure 3).

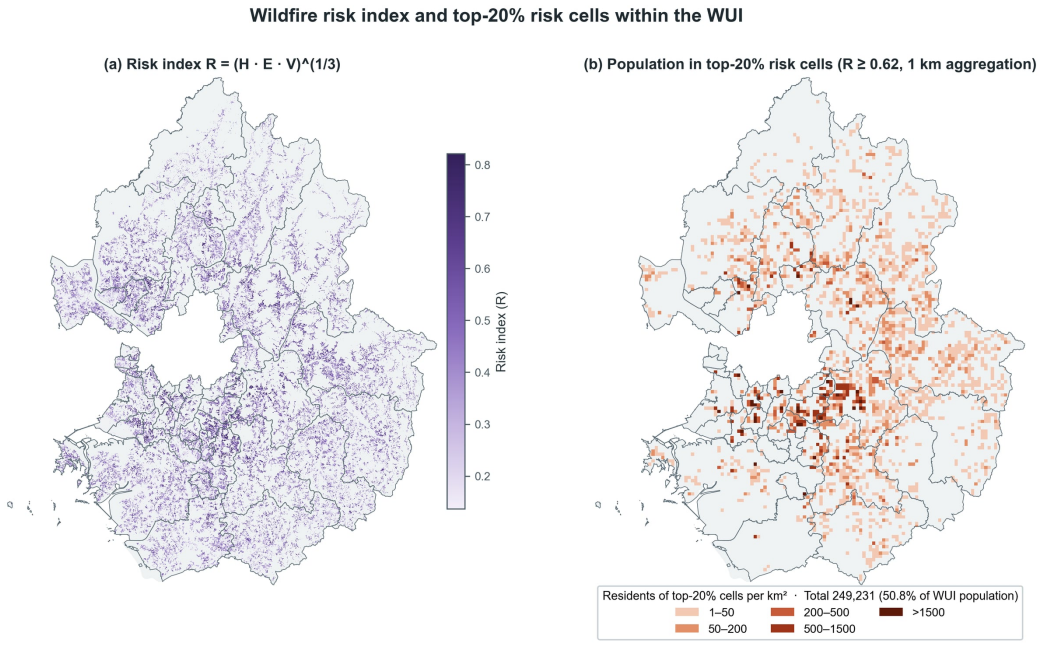


Figure 3. Risk index R (**a**) and population living in top-20% risk cells (**b**). Panel (**b**) is aggregated to 1 km for display. The threshold R ≥ 0.62 is the 80th percentile among WUI cells with R > 0.

4.4. Response Capacity Proxies Are Uneven and Higher in Densely Populated Municipalities

Detection, suppression access, and evacuation travel time are reported first, followed by their relationship to risk and urbanization.

4.4.1. Detection

The 237 operational cameras cover 65.2% of the WUI population (Figure S3). Adding the towers and posts located from lot numbers raises this to an upper bound of 70.6%. Gapyeong and Yangpyeong hardly gain, because the source data contain no towers or posts in these two counties. In some municipalities, cameras recorded as broken or aging in the February 2026 inventory were excluded, so their coverage depends partly or wholly on cameras in neighboring municipalities. Coverage by municipality is given in Table S1, and coverage by camera status in Text S1.

4.4.2. Suppression Access and Its Relation to Suppression Records

WUI cells lie a median 9.3 km from the 35 fire stations, and road-weighted travel times from the stations order municipalities almost identically (Section 3.5; Table S1).

The suppression records show weak associations with this proxy in the expected direction (Table S6). Among the 1249 fires linked to their parcels, fire-station distance correlated with the time from ignition to containment of the main fire at Spearman +0.095 and with burned area at +0.150; in a log-linear model, its association with containment time disappeared once burned area was controlled.

Fires in camera viewsheds were smaller but were not contained faster. At the municipal level, C was related to the share of fires of 1 ha or more but not to containment time (Table S6). The register holds no detection times, so the detection component could not be tested.

4.4.3. Evacuation Travel Time

With roads at 40 km/h, the median travel time from WUI cells is 3.1 min to base shelters, 5.2 min to strict shelters, and 5.7 min to civil-defense shelters. In the 28 municipalities with

complete road data, 90.4% of the WUI population reach a strict shelter within 15 min (Figure 4a).

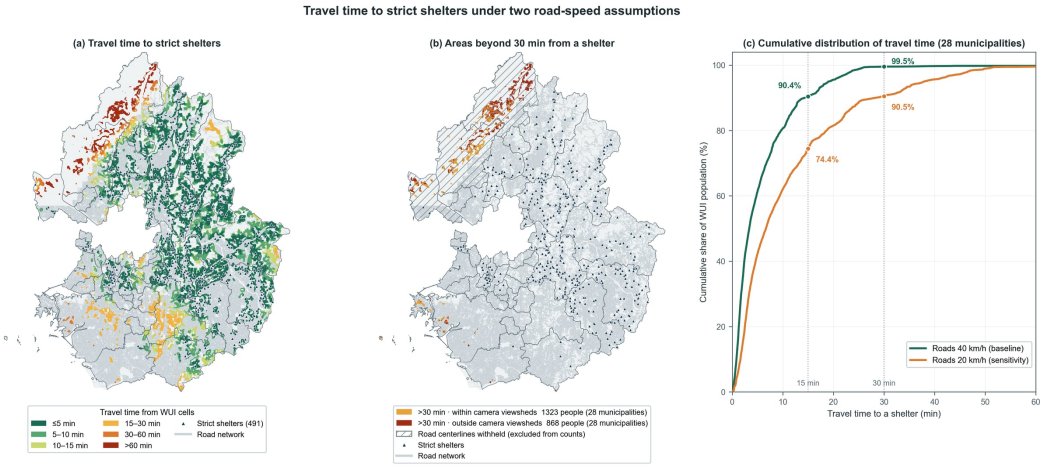


Figure 4. Travel time to strict shelters (**a**) and areas beyond 30 min (**b**), both with roads at 40 km/h, and the cumulative distribution of travel time (**c**). Multi-source Dijkstra on a road-weighted grid (roads 11.1 m/s, non-road cells 1.1 m/s, 8-neighbor grid). In (**b**), orange and red mark areas beyond 30 min within and outside the viewsheds of operational cameras (1323 and 868 people); population counts in the legend cover the 28 municipalities with complete road data, and province-wide values are given in Section 4.5. Road centerlines are withheld in parts of Yeoncheon, Paju, and Gimpo (northwest), where travel times are overestimated. Gray hatching in (**b**) marks those three municipalities, which are excluded from the counts. Panel (**c**) gives the share of the WUI population of the remaining 28 municipalities that reaches a strict shelter within a given time, at 40 and 20 km/h on roads; the gap between the two curves is the sensitivity of the result to the speed assumption.

At 20 km/h this share falls to 74.4%, and the population beyond 30 min rises from 2191 to 44,567, mainly in Yongin, Hwaseong and Siheung (Figure 4c; Table 5). These values are lower bounds that exclude warning, preparation, and departure delays (Section 3.6.2).

Table 5. WUI population by travel time to strict shelters and population outside camera viewsheds (two road-speed assumptions). The 28 municipalities exclude Yeoncheon, Paju and Gimpo, where road centerlines are withheld.

Travel Time	Roads 40 km/h	of Which Outside Camera Viewsheds	Roads 20 km/h	of Which Outside Camera Viewsheds
28 municipalities (WUI population 469,388)				
≤15 min	424,276 (90.4%)	145,380	349,407 (74.4%)	127,970
15–30 min	42,921 (9.1%)	14,191	75,414 (16.1%)	17,706
>30 min	2191 (0.5%)	868	44,567 (9.5%)	14,763
All 31 municipalities (WUI population 490,984)				
≤15 min	432,777 (88.1%)	149,201	351,867 (71.7%)	129,293
15–30 min	44,664 (9.1%)	15,125	82,245 (16.8%)	20,766
>30 min	13,543 (2.8%)	6724	56,872 (11.6%)	20,991

4.4.4. Capacity, Risk and Urbanization

Across the 31 municipalities, C and EC correlate with R at +0.846 and +0.485 and with population density at +0.818 and +0.458; controlling for density weakens the correlations with R to +0.551 and +0.221 (Table S7; Figure S4).

Allowing for the spatial clustering of municipal values (Text S1.5) reduces the effective sample size to about 9 for C–R and 16 for EC–R, and the EC–R interval then includes zero. With all three indices averaged over WUI cells, the correlations become negative (C–R −0.154, EC–R −0.209; Text S1.5). Gwangju, Yongin, Yangpyeong and Gapyeong, which are among the municipalities with the largest WUI populations, fall below the municipal means of both capacities.

4.5. Public Shelter Data Offer No Wildfire Destinations and Little Above-Ground Capacity

The audit of evacuation facilities identifies three gaps—in designation, suitability, and listed capacity (Sections 4.5.1–4.5.3)—after which travel time and detection are crossed (Section 4.5.4) and facilities within the scope of the national guideline are examined (Section 4.5.5).

4.5.1. Designation

In public shelter data, the multi-purpose designation fields of landslide shelters list 34 civil-defense, 93 chemical-accident, and 301 temporary-housing designations but no wildfire category. This refers to the designation fields in public data and does not rule out wildfire evacuation sites that municipalities operate outside those data.

4.5.2. Suitability

Of the 4052 civil-defense shelters in regular operation, 4047 (99.9%) are underground. Their combined maximum capacity, 50.99 million, is 104 times the WUI population.

4.5.3. Listed Capacity

The listed (nominal) capacity of potential above-ground destinations under the base definition is 86,987, or 18% of the WUI population; strict shelters alone list 40,615 places (8%). These are maximum numbers recorded in the shelter data, not capacities verified for wildfire use. One base shelter with 50 places lies outside the 100 m grid, so the travel-time and load analyses use 86,937 places. No landslide shelters are listed for Osan, so its listed above-ground capacity is zero. The 18% assumes that every WUI resident heads for a public shelter.

When every WUI cell is assigned to its fastest-reached base shelter, 782 of the 917 shelter locations that receive anyone are assigned more people than they list, and they receive 97.9% of the WUI population; the median shelter location is assigned 6.55 times its listed capacity. The summed excess of assigned population over listed capacity is 438,732 people, 89.4% of the WUI population, against the shortfall of 82.3% implied by the 18% total, so the location of capacity adds about seven percentage points. Under the strict definition, the excess is 94.2% (Table S6). Because people turned away were not reassigned, these figures describe the mismatch between where capacity is listed and where people live, not the outcome of a capacity-constrained evacuation.

4.5.4. Distance and Detection

WUI population by travel-time class, crossed with camera coverage under both road-speed assumptions, is given in Table 5.

In the 28 municipalities with complete road data, the population beyond 30 min at 40 km/h numbers 2191, almost all in Hwaseong (1094) and Ansan (1059); at 20 km/h it

numbers 44,567 (Section 4.4). Province-wide values also include Paju (6123), Yeoncheon (3438) and Gimpo (1791) at 40 km/h (Figure 4b), with median travel times from WUI cells of 35, 81 and 49 min where road centerlines are withheld and, in Yeoncheon, no shelter can host temporary stays.

The 868 people in the 28 municipalities who need more than 30 min to reach a strict shelter and live outside camera viewsheds face both deficits (14,763 at 20 km/h; province-wide, 6724 and 20,991).

Of the WUI population, 6.7% lives within 2 km of the outer provincial boundary, against 15.1% of the 13,543 people province-wide beyond 30 min at 40 km/h, mainly in Ansan, Hwaseong and Gimpo and partly along the coast (Text S1).

4.5.5. Facilities Within the Scope of the National Guideline

Of the 2140 elderly medical-welfare facilities, 783 (31,624 residents) lie within 100 m of a forest boundary (Zone I) and 1404 (51,430 residents) within 300 m (Zone II), so 70.5% of residents fall within the guideline's scope (province-wide counts; two facilities with 81 residents lie outside the municipal boundary grid, so they are absent from the municipal sums in Table S1 and, lacking travel times and camera visibility, from the counts below); 172 of 294 long-term care hospitals (58.5%) also lie in Zone II. Only 254 of the 2140 facilities lie in WUI cells, because the guideline considers distance to any forest, whereas the WUI requires a high forest share or a large vegetation patch.

The median travel time from Zone II facilities is 5.8 min (11.3 min at 20 km/h). In the 28 municipalities with complete road data, 864 residents (30 facilities) need more than 30 min at 40 km/h and 8286 (194 facilities) at 20 km/h, mainly in Hwaseong (3357) and Yongin (1884); province-wide the figures are 3344 and 11,153. Province-wide, 12,393 residents (361 facilities) are outside operational camera viewsheds, mainly in Hwaseong, Namyangju, Pyeongtaek and Yangpyeong, and in the 28 municipalities, 80 facilities with 3130 residents are both more than 30 min away at 20 km/h and outside camera viewsheds.

4.6. Camera-Coverage Gaps Concentrate in Forested Counties and Travel-Time Gaps in Peri-Urban Cities

The two axes are combined in the two ways described in Section 3.1. Top-20% risk cells are crossed with the two deficits measurable per cell—travel time to a strict shelter beyond 30 min and location outside operational camera viewsheds—and municipalities are placed in quadrants by the medians of population-weighted R and of C or EC (Figure 5; Table S8).

In the 28 municipalities with complete road data, 242,934 people live in top-20% risk cells. Of them, 57,778 (23.8%) live outside the viewsheds of operational cameras, 910 are more than 30 min from a strict shelter at 40 km/h and 23,970 at 20 km/h, 6473 face both deficits at 20 km/h, and 75,275 (31.0%) face at least one (province-wide 249,231, 60,153, 26,271, 7398 and 79,026). The two deficits are spatially distinct (Figure 5c). Detection gaps concentrate in the forested east and north: of the 12,086 people in top-20% cells in Yangpyeong, 85% live outside camera viewsheds, against 55% in Gapyeong, 52% in Pocheon, and practically all in Yeoju. Gwangju alone contributes 14,204 people, 31% of its top-20% population. Travel-time gaps at 20 km/h concentrate in Yongin (9478) and Hwaseong (7218), where the two deficits also overlap most (1768 and 2460 people).

At the municipal level, which adds shelter capacity, 16 municipalities lie at or above the median of R, with Namyangju exactly at it. Two—Gwangju and Namyangju, with 117,938 WUI residents (24.0%)—fall below the median of C, and five—Gwangju, Siheung, Ansan, Osan and Gwangmyeong, with 110,981 (22.6%)—fall below the median of EC. Six municipalities with 143,051 WUI residents (29.1%) are in at least one high-risk·low-response quadrant, and one of them is in both. The low-risk·low-response quadrant contains sev-

eral of the largest but most dispersed WUI populations—Yongin, Yangpyeong, Gapyeong, Hwaseong, Paju and Goyang among them—with 39% (EC) to 48% (C) of the WUI population. Four of them—Yangpyeong, Gapyeong, Yongin and Hwaseong—nevertheless appear among the cell-level deficits described earlier in this section.

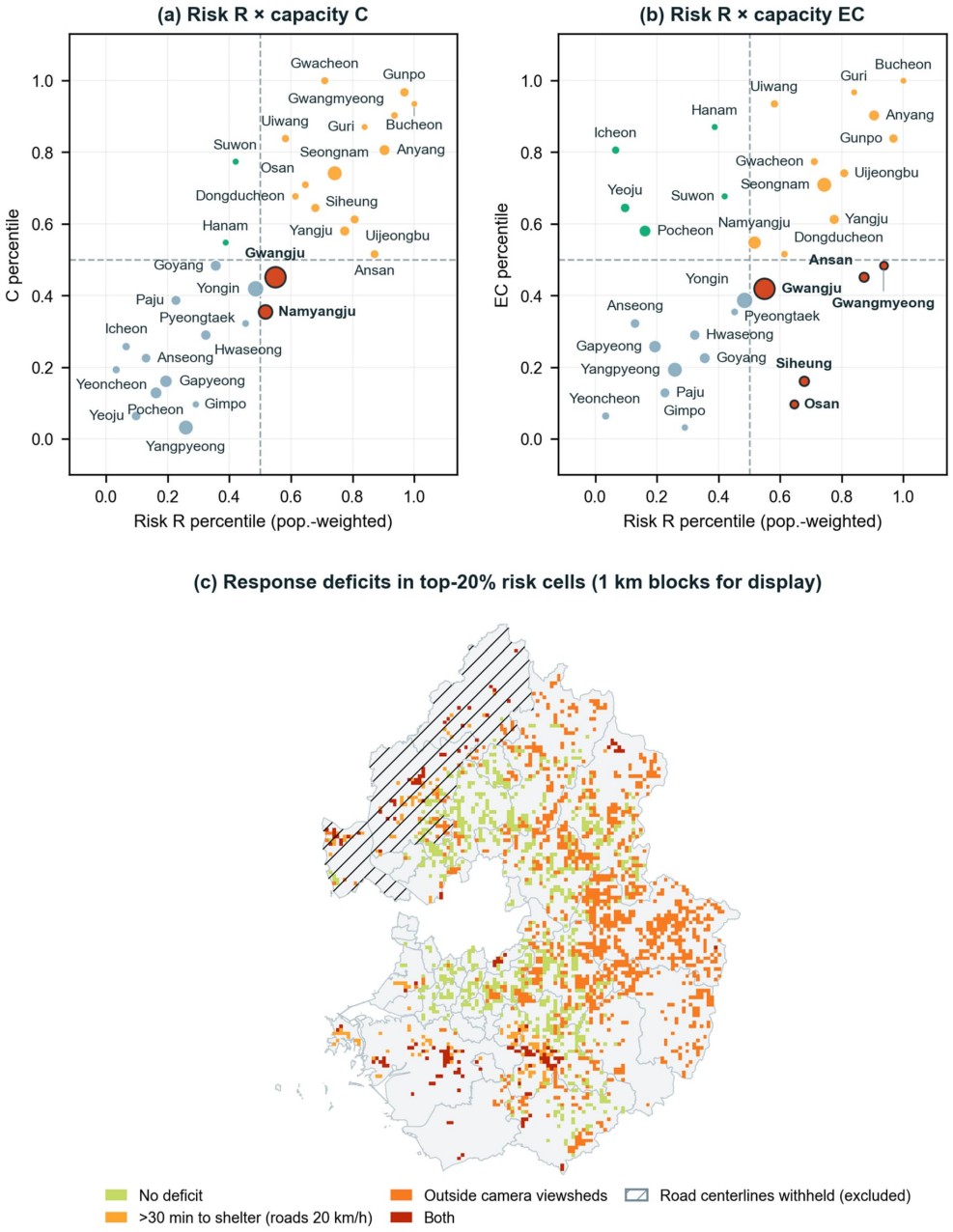


Figure 5. Risk–response mismatch. (**a**) Municipal risk R (population-weighted percentile) against suppression and detection capacity C and (**b**) against evacuation capacity EC, split at the medians of the baseline indices (dashed lines); circle area is WUI population and high-risk·low-response municipalities are shown in red with bold labels. Other circle colors mark the remaining quadrants: orange, high risk–high capacity; green, low risk–high capacity; blue-gray, low risk–low capacity. Thin lines connect labels placed away from their circles. Membership near the medians changes under alternative indices (Table S9). (**c**) Response deficits in top-20% risk cells, aggregated to 1 km blocks for display: beyond 30 min from a strict shelter at 20 km/h, outside operational camera viewsheds, or both. Hatching marks the three border municipalities with withheld road centerlines, which are excluded from the counts.

These quadrants are defined by the baseline indices and median thresholds. Gwangju's population-weighted risk is at the 55th percentile and Namyangju's at the median. Across all combinations of risk and capacity indices (Section 4.7), Gwangmyeong and Siheung remained high-risk·low-EC in every case, Osan, Ansan, and Dongducheon in 60–75% of cases, and Gwangju and Namyangju in 25% or fewer for either capacity (Table S9). Yongin, just below the median of R at baseline, and Goyang entered a high-risk·low-response quadrant in 40–50% of combinations, all using the arithmetic mean.

4.7. Where Deficits Lie Is Robust; Their Size and Municipal Classes Are Less So

The sensitivity analyses test whether the places and people identified depend on thresholds, weights, aggregation rules, or grid size. Results are summarized in Table 6 and Figure S5, with details in Tables S9 and S10. Municipal rankings are robust to the weights of the risk index and to most WUI thresholds, but not to the 2.4 km interface distance or to an arithmetic mean averaged over WUI cells.

Two arithmetic-mean scenarios rank different sets of cells. Over all WUI cells, the arithmetic mean is positive even where hazard or vulnerability is zero, so its top 20% is a much larger set with a different denominator (60,327 cells rather than 7077). Over the same cells as the baseline, it retains 92.5% of the baseline top-20% population, the deficit populations change by less than 5%, and the same municipalities lead both deficits (Table S10). Under the arithmetic mean, Goyang and Yongin enter the high-risk·low-response quadrants and Gwangju and Namyangju leave them.

With hazard as ignition probability alone, 92.8% of the baseline top-20% population is retained, and the cell-level deficits change by less than 3%, with the same leading municipalities. At the municipal level, Gwangju, Namyangju and Osan fall just below the median of R, and Pyeongtaek, Suwon and Hanam rise above it.

Alternative weights of C leave the high-risk·low-C quadrant unchanged, whereas those of EC change quadrant membership near the median (Table 6). Across all combinations of risk and capacity indices, Gwangmyeong and Siheung are high-risk·low-EC in every case, and Gwangju and Namyangju in a minority (Table S9). On coarser grids, the share of the top-20% population beyond 30 min hardly changes, whereas the share outside camera viewsheds falls from 23.8% at 100 m to 17.3% at 1 km, with largely the same leading municipalities (Text S1.7).

At the cell level, R correlates more strongly with E (Spearman +0.675) than with H or V (Text S1). The population facing evacuation difficulty depends on road speed but hardly on off-road walking speed (Table 6).

Table 6. Sensitivity results (Spearman rank correlation of municipal rankings with the baseline unless otherwise noted).

Target	Change	Result
WUI density threshold	3.09/12.35 households/km^2	1.000; WUI population 3.5%/3.5%
WUI vegetation threshold	0.4/0.6	0.969/0.960; WUI population 7.3%/1.9%
WUI window size	500 m/2 km	0.945/0.950; WUI population 2.9%/4.7%
WUI interface distance	1 km	0.933; WUI population 5.7%
WUI interface distance	2.4 km (Radeloff)	0.750; WUI population 27.1%
Risk index weights	H ×2/V ×2/PCA	0.999/0.997/0.995
Risk index aggregation	INFORM-type four-component $(H \cdot E \cdot V \cdot (1-C))^{(1/4)}$	0.894
Risk index aggregation	Arithmetic mean over all WUI cells	0.215 (municipal means over WUI cells); 0.966 (population-weighted, as used in Section 4.6); top 20% = 60,327 cells instead of 7077 (different denominator): Jaccard 0.117, 390,100 people in 28 municipalities
Risk index aggregation	Arithmetic mean over the baseline cells (all three components positive)	0.998 (WUI-cell means); 0.970 (population-weighted); top-20% cells: Jaccard 0.694, 92.5% of baseline top-20% population retained
Hazard without spread potential	H = ignition probability only	0.992 (WUI-cell means); 0.965 (population-weighted); top-20% cells: Jaccard 0.820, 92.8% of population retained
Risk index without E	$(H \cdot V)^{(1/2)}$	0.548; four of the top five municipalities shared
V weights (Spearman across Gyeonggi cells)	Equal weights for four components	0.987
V weights (Spearman across Gyeonggi cells)	Excluding older adults and housing type	0.763
V weights (Spearman across Gyeonggi cells)	Unweighted facility counts	0.753
V weights (Spearman across Gyeonggi cells)	Excluding housing type	0.987
Spread potential weights	Equal weights	0.998
C weights (camera:fire station)	0.3:0.7/0.7:0.3	0.990/0.990; high-risk·low-C quadrant unchanged
EC weights (travel time:camera:capacity)	Equal/0.6:0.2:0.2/0.2:0.2:0.6	0.982/0.930/0.859; quadrant membership changes (Table S9)
EC without camera visibility	0.62:0:0.38	0.933; C–EC correlation 0.588 → 0.339

Table 6. *Cont.*

Target	Change	Result
Grid resolution of deficits (28 municipalities)	200 m/500 m/1 km blocks	Outside camera viewsheds 22.2/20.9/17.3% of top-20% population (23.8% at 100 m); beyond 30 min at 20 km/h 8.9/9.6/8.9% (9.9%); municipal rankings of both deficits ≥0.957
Travel speed	Roads 20 km/h	28 municipalities: within 15 min 90.4% → 74.4%, >30 min 2191 → 44,567; province-wide: 88.1% → 71.7%, 13,543 → 56,872
Off-road walking speed	0.79 m/s (older adults)	28 municipalities: >30 min 2196 (40 km/h) and 44,751 (20 km/h); within 15 min 90.4% and 73.6%
Border municipalities	Excluding Yeoncheon, Paju and Gimpo (n = 28)	C–R 0.831 (partial 0.556); EC–R 0.391 [−0.01, 0.70] (partial 0.143)
Shelter open/closed field	Excluding 158 shelters recorded as not open	Listed above-ground capacity 16%; >30 min in 28 municipalities 9270 (40 km/h) and 65,055 (20 km/h)
Camera status	250/237/223 cameras	WUI population coverage 66.4/65.2/63.4%; with towers and posts 71.6/70.6/69.4%
Observer height	5–40 m	≥0.987; absolute coverage varies by 9.7 percentage points
Data corrections	Before vs. after T1 reclassification, facility de-duplication and camera filtering	R 0.999, V 0.998, C 0.995, EC 0.998

5. Discussion

5.1. Spatial Mismatch Between Risk Conditions and Response Capacity

Mapping risk conditions and response capacity as separate axes reveals local deficits that a ranking by a composite index would hide. In Gyeonggi, response capacity was positively correlated with risk conditions (C–R + 0.846), but this is weak evidence that resources were allocated according to risk. The association weakens once population density is taken into account, and it disappears when municipal values are averaged over WUI cells instead of being weighted by population (Sections 4.4 and 4.7). Fire stations, monitoring cameras and WUI residents are all concentrated in urbanized areas, and municipal data cannot separate these effects. The main evidence of this study therefore lies not in correlations among municipalities but in the cells where high-risk conditions and low response capacity coincide.

The location of these cells was largely stable across analytical choices, whereas the size of the deficits and the municipal classes were less so. When the same top-20% WUI cells were compared, the deficit estimates changed by less than 5% under the arithmetic mean and an ignition-only hazard, and the leading municipalities were largely the same on grids of up to 1 km. An arithmetic mean computed over all WUI cells instead ranks a different and much larger set of cells and therefore identifies a different high-risk population rather than testing the stability of the baseline (Section 4.7). The size of the deficits varied more: the share of the top-20% population outside camera viewsheds fell from 23.8% at 100 m to 17.3% at 1 km, and the top-20% population beyond 30 min from a shelter ranged from 910 to 23,970 depending on road speed. Membership of the high-risk·low-response quadrants was more sensitive: it changed with the aggregation rule of the risk index, the hazard specification, and the weights of EC, mainly for municipalities near the medians, and only Gwangmyeong and Siheung remained high-risk·low-EC under every combination (Section 4.7; Table S9). The cell-level deficits themselves do not depend on the weights of C and EC. The location of cell-level deficits can therefore guide field inspections, but deficit populations should be read as assumption-dependent ranges and municipal classes as supporting information, and priorities for individual municipalities should be set with caution.

5.2. Suitability and Accessibility of Evacuation Destinations

Public shelter data contain no wildfire designation. Almost all civil-defense shelters with recorded capacity are underground, and the listed capacity of the potential above-ground destinations selected here equals 18% of the WUI population (Section 4.5). These findings describe the composition of public inventories and their nominal capacity. They do not show that municipalities have no local destinations outside these data, nor that the selected above-ground facilities are suitable for wildfire evacuation. The national standard messages for mobile disaster alerts point the same way: the wildfire evacuation message leaves the destination blank, to be filled in when the alert is sent, whereas the landslide message refers to a designated shelter [71]. The template thus leaves the destination to be specified during an event rather than drawing it from a prepared list. This combination—a large designated inventory that does not serve the hazard in question—can be diagnosed elsewhere in four steps: compiling the inventory, classifying each facility as suitable or unsuitable for the hazard, comparing the capacity of suitable facilities with the exposed population, and computing travel times over a range of speeds. The nearest-shelter load, in which the population assigned in excess of listed capacity equals 89.4% of the WUI population, likewise depends on its assumptions and indicates capacity pressure rather than the outcome of a capacity-constrained evacuation.

Short travel times alone do not establish that evacuation is feasible. When roads operate at the assumed speed, 90.4% of the WUI population in the 28 municipalities can reach a shelter able to host temporary stays within 15 min, but actual evacuation also depends on warning and departure times, means of transport, traffic, and the suitability and capacity of the destination [41,43,72–74]. Advance transport plans are particularly important for facility residents who cannot move on their own. The 2025 wildfires in southeastern Korea, in which older adults and nursing-home residents died [27–29], and the national standards that call for advance evacuation of vulnerable groups [31–33] show the need to decide in advance not only when to leave but also where to go and by what means.

Designation of destinations can begin with existing facilities. Schools, village halls, gymnasiums and open spaces have been used for this purpose abroad [75–79], but the existence of a facility does not make it suitable for wildfire evacuation. Separation from forest, the safety of buildings and outdoor spaces, access routes, the time people can stay, and the ability to receive vulnerable people need to be assessed facility by facility. The maps produced here can identify where such assessments should start. The two deficits follow different settlement patterns: detection gaps affect the largest shares of residents in sparsely settled, extensively forested counties and the largest numbers in cities with extensive forest-edge settlement, whereas travel-time gaps arise mainly in peri-urban areas, where travel times lengthen most when roads slow (Section 4.6). Monitoring coverage is therefore the first concern in the former, and access to shelters and advance transport in the latter. The aim is less to build new facilities or install new equipment than to check whether existing resources and local plans actually reach the residents concerned.

5.3. Methodological Implications and Limitations

The extent of the WUI should match the purpose of a study and the regional landscape. Applied to Gyeonggi, the 2.4 km interface distance developed for the western United States multiplies the exposed population eightfold relative to our definition, largely by adding residents of high-rise apartments. In this study, the size of the WUI population was sensitive to the interface distance and the vegetation-share threshold, and municipal rankings were sensitive mainly to the interface distance (Section 4.7). Analyses of the evacuation of forest-adjacent residents and analyses of long-distance spotting therefore should not adopt the same WUI boundary by default, but report a distance suited to their purpose together with its consequences [38,39].

The maps are a regional screening tool. The hazard surface is static and simulates neither daily wind nor fire spread, so it complements rather than replaces daily fire danger forecasting [80]. It represents human-caused ignition only; smoldering ignitions that persist in moist duff or litter and are hard for cameras to detect are represented only when they were reported; and its spread component is an expert-based term that was not statistically validated. The geometric mean makes R depend strongly on exposure, so it largely ranks where many people live near forests (Section 4.7). Population, older-adult, and land-cover data refer to different dates; the residential population grid does not represent daytime populations at work or school; and the older-adult share ranges from 18.0% to 28.2% depending on the value assigned to suppressed cells. Camera viewsheds are proxies for automated monitoring under simplified terrain and viewing conditions, and fire-station distance is not response time. Travel times exclude road closures, congestion, departure delays, and shelters outside the province, and the wildfire suitability and listed capacity of candidate facilities were not verified in the field. Road data are incomplete in parts of three border municipalities. Conversely, the WUI definition excludes urban residents next to small forests, so the deficits of vulnerable facilities and residents are conservative. Municipal relationships were estimated from 31 spatially dependent units and should be

read as descriptive associations. Finally, the 100 m grid is the resolution at which results are reported, not the accuracy with which the location of individual cells or response performance was established.

The consequences of these limitations differ among results. The absence of a wildfire designation, the share of underground shelters, and listed capacity are structural findings obtained directly from the data. The population size of detection and travel-time deficits and the nearest-shelter scenario are spatial estimates that depend on model assumptions. That detection would be slower or evacuation harder in these places during an actual fire is a planning hypothesis that requires validation against operational records. Above all, this study did not measure detection times, suppression outcomes, or evacuation success in actual fires, nor did it estimate expected losses to people, property, or ecosystems (Section 3.1). A record of mostly small fires does not show that the evacuation system would be adequate in a large fire, and the proxies used here cannot by themselves establish actual response failure or the size of residual risk.

5.4. Future Research

The next step is to compare the spatial proxies with operational records and field surveys. Actual detection times and camera status, and dispatch and arrival records of suppression crews, are needed to validate the detection and suppression indicators. Evacuation analyses should incorporate road closures and congestion, departure delays, the reassignment of residents according to shelter capacity, and movement across municipal and provincial boundaries [44,66]. Field assessment of the structure, forest separation, and operability of candidate facilities would narrow the list of potential destinations to one that can be used in actual plans. Coupling the static hazard surface with daily weather and fire-spread simulation, and applying the same procedure to regions with different settlement patterns, would help establish how far this analysis can be transferred.

6. Conclusions

This study mapped wildfire risk conditions and spatial proxies of response capacity on a 100 m grid for Gyeonggi Province and examined where high risk conditions coincide with low response capacity. The most certain findings, because they rest directly on inventory counts, concern evacuation destinations. Public shelter data contain no wildfire designation, 99.9% of civil-defense shelters in use are underground, and the listed capacity of potential above-ground destinations would cover 18% of the WUI population if every resident went to a public shelter. These figures rest on public facility lists and on the WUI definition of this study, so they do not rule out local destinations that the lists do not record. If every resident went to the nearest shelter, the population assigned in excess of listed capacity would equal 89.4% of the WUI population; because people exceeding capacity were not reassigned to other shelters, this figure indicates capacity pressure rather than the result of a capacity-constrained evacuation analysis. Wildfire destinations should therefore be designated in advance, with the suitability and actual capacity of each facility verified, and where existing facilities prove suitable, indoor shelters and outdoor refuges could be designated together. The need is greatest for residents who cannot evacuate on their own. WUI residents are older than the provincial population, and 70.5% of the residents of elderly medical-welfare facilities live within 300 m of any forest patch (the guideline's criterion), so advance transport plans for these facilities should specify the means of transport, the designated destination and the route.

Beyond the destinations themselves, the analysis located where people in high-risk conditions have the least access to detection and shelters. In the 28 municipalities with complete road data, 242,934 people live in the top 20% of WUI cells with positive risk

($R \geq 0.62$). Of them, 57,778 live outside camera viewsheds and 23,970 are more than 30 min from a shelter able to host temporary stays when roads slow to 20 km/h. Where these deficits lie was largely stable across analytical choices: compared on the same cells, results under the arithmetic mean and an ignition-only hazard differed by less than 5%, and the leading municipalities were largely the same on grids of up to 1 km. Their size, by contrast, depended on grid size and road speed: the share outside camera viewsheds fell from 23.8% at 100 m to 17.3% at 1 km, and travel-time deficits depended on the assumed road speed. Monitoring coverage should therefore be examined first in sparsely settled, extensively forested counties and in cities with extensive forest-edge settlement, and shelter access and advance transport in peri-urban areas where travel times lengthen most when roads slow.

The municipal results are less secure than the location of these cell-level deficits. Membership of the high-risk·low-response quadrants changed with the aggregation rule of the risk index, the hazard specification and the weights of EC, mainly for municipalities near the median thresholds, and the association between risk conditions and response capacity could not be separated from urbanization or from the way municipal values are aggregated. Priorities for individual municipalities should therefore be set with caution, using municipal rankings together with the size of the exposed population and the cell-level deficits, and correlations alone should not be used to judge whether response resources were allocated according to risk. The response indices are themselves spatial proxies: the suppression component agrees only weakly with suppression records, the detection component could not be checked against any record, and none of the indices represents the actual performance of detection, suppression and evacuation. Nor does a record of frequent but mostly small fires show that the evacuation system would be adequate in a large fire. The places where high-risk conditions coincide with low response capacity should therefore be verified in the field, and the explanatory power of the indicators tested against operational records.

By mapping risk conditions and response capacity separately, this study provides a basis for designating wildfire destinations and verifying their suitability, for advance transport planning for vulnerable residents next to forests, and for field inspection of places with low detection and evacuation access. Applying the same analysis to rural regions with settlement patterns different from Gyeonggi, and examining the suitability and accessibility of shelters for other hazards such as floods, are tasks for future research.

Supplementary Materials: The following supporting information can be downloaded at: https://www.mdpi.com/article/10.3390/ijgi15110511/s1, Text S1: supplementary methods and results (record-level data processing, viewsheds of lookout towers and guard posts, full specification of the sensitivity analyses and detailed results). Figure S1: annual number and burned-area distribution of the 1272 wildfires in the register. Figure S2: the three components of the risk index (hazard, exposure and vulnerability). Figure S3: wildfire detection viewsheds of operational cameras and the upper-bound estimate with lookout towers and guard posts. Figure S4: population density against suppression and detection capacity and evacuation capacity. Figure S5: sensitivity of the WUI, the risk index, and viewsheds. Table S1: municipal summary for the 31 municipalities. Table S2: coefficients of the case–control ignition model. Table S3: statistical diagnostics. Table S4: percentile transformations used in the indices. Table S5: analysis scripts, their run times and main outputs. Table S6: operational check of the suppression and detection proxy against suppression records, and nearest-shelter load. Table S7: relationships between capacity and risk at the municipal level. Table S8: risk–response mismatch by municipality. Table S9: frequency of high-risk·low-response quadrant membership across alternative indices. Table S10: robustness of the results to alternative risk indices, weights of the response indices, block aggregation and the aggregation of municipal values.

Author Contributions: Conceptualization, Miyeon An and Dongwoo Kim; methodology, Miyeon An; software, Miyeon An; validation, Miyeon An and Yunwon Choi; formal analysis, Miyeon An; investigation, Miyeon An and Yunwon Choi; resources, Dongwoo Kim; data curation, Miyeon An and Yunwon Choi; writing—original draft preparation, Miyeon An; writing—review and editing,

Yunwon Choi and Dongwoo Kim; visualization, Miyeon An; supervision, Dongwoo Kim; project administration, Dongwoo Kim; funding acquisition, Dongwoo Kim. All authors have read and agreed to the published version of the manuscript.

Funding: This research was supported by the Gyeonggi Provincial Government through two policy research projects commissioned to the Gyeonggi Research Institute (GRI), Republic of Korea: A Study on Spatial Planning and Risk Management Strategies for Areas Vulnerable to Forest-Related Disasters in Gyeonggi-do (Policy Research 2026-41) and Research on Strategies for Promoting Ecological Restoration in Gyeonggi-do: Focused on Identifying Ecological Restoration Sites (Policy Research 2024-83). The APC was funded by the authors.

Institutional Review Board Statement: Not applicable.

Informed Consent Statement: Not applicable.

Data Availability Statement: The analysis code and the municipal-level summary tables supporting the findings of this study are openly available in Zenodo at https://doi.org/10.5281/zenodo.23664110. The wildfire register and the inventory of wildfire prevention and suppression equipment supplied by the Gyeonggi Provincial Government, and the ignition parcels derived from the register, cannot be made public because the records identify individual privately owned cadastral parcels; summaries at a level that does not identify individual parcels are available from the corresponding author on reasonable request with the permission of the data provider. The remaining datasets—the SGIS population, household and housing grids, the National Land Statistics older-adult grid, the Urban Ecological Status Map, the forest type map, the continuous cadastral map, the continuous digital topographic map, civil-defense shelters, landslide-vulnerable-area shelters, and the vulnerable-facility and school lists published on Gyeonggi Data Dream (https://data.gg.go.kr (accessed on 11 September 2026))—are available from their public providers.

Acknowledgments: During the preparation of this manuscript, the authors used Claude Opus 5.5 (Anthropic) for the purposes of language editing and of revising and tidying the analysis code. The authors have reviewed and edited the output and take full responsibility for the content of the publication.

Conflicts of Interest: The authors declare no conflicts of interest.

References

1. Tang, W.; He, C.; Emmons, L.; Zhang, J. Global expansion of wildland-urban interface (WUI) and WUI fires: Insights from a multiyear worldwide unified database (WUWUI). *Environ. Res. Lett.* **2024**, *19*, 044028. [CrossRef]
2. Torres-Vázquez, M.Á.; Dalle Vaglie, M.; Kettridge, N.; Martellozzo, F.; Miguez-Macho, G.; Provenzale, A.; Royé, D.; Randelli, F.; Turco, M. Assessing decadal changes in human exposure near wildfires in a Mediterranean region. *Sci. Rep.* **2026**, *16*, 5827. [CrossRef] [PubMed]
3. Guo, Y.; Wang, J.; Ge, Y.; Zhou, C. Global expansion of wildland-urban interface intensifies human exposure to wildfire risk in the 21st century. *Sci. Adv.* **2024**, *10*, eado9587. [CrossRef] [PubMed]
4. Schug, F.; Bar-Massada, A.; Carlson, A.R.; Cox, H.; Hawbaker, T.J.; Helmers, D.; Hostert, P.; Kaim, D.; Kasraee, N.K.; Martinuzzi, S.; et al. The global wildland–urban interface. *Nature* **2023**, *621*, 94–99. [CrossRef] [PubMed]
5. Radeloff, V.C.; Mockrin, M.H.; Helmers, D.; Carlson, A.; Hawbaker, T.J.; Martinuzzi, S.; Schug, F.; Alexandre, P.M.; Kramer, H.A.; Pidgeon, A.M. Rising wildfire risk to houses in the United States, especially in grasslands and shrublands. *Science* **2023**, *382*, 702–707. [CrossRef] [PubMed]
6. Zhang, X.; Liang, L. Wildfire as urban risk: Global synthesis of compound hazards, cascade pathways, and research-exposure-vulnerability mismatch. *Environ. Res. Lett.* **2026**, *21*, 133007. [CrossRef]
7. Steinmann, C.B.; Koh, J.; Scholten, R.C.; Bresch, D.N.; Hantson, S. A survival guide for assessing global fire risks to natural and human systems. *Int. J. Disaster Risk Reduct.* **2026**, *140*, 106140. [CrossRef]
8. IPCC. Summary for Policymakers. In *Climate Change 2014: Impacts, Adaptation, and Vulnerability. Part A: Global and Sectoral Aspects. Contribution of Working Group II to the Fifth Assessment Report of the Intergovernmental Panel on Climate Change*; Field, C.B., Barros, V.R., Dokken, D.J., Mach, K.J., Mastrandrea, M.D., Bilir, T.E., Chatterjee, M., Ebi, K.L., Estrada, Y.O., Genova, R.C., et al., Eds.; Cambridge University Press: Cambridge, UK, 2014; pp. 1–32. [CrossRef]

9. Marin-Ferrer, M.; Vernaccini, L.; Poljansek, K. *Index for Risk Management INFORM: Concept and Methodology Report—Version 2017*; EUR 28655 EN; Publications Office of the European Union: Luxembourg, 2017. [CrossRef]
10. Shafiq, Y.; Muhammad, A.; Noor, S.; Kumar, K.; Chhipa, U.e.A.; Valente, M.; Razzak, J.; Ragazzoni, L.; Barone-Adesi, F.; Pham, P. The modification of risk assessment ranking when considering the female population and children in the INFORM risk index for selected countries. *Sci. Rep.* **2025**, *15*, 26527. [CrossRef] [PubMed]
11. United Nations General Assembly. *Report of the Open-Ended Intergovernmental Expert Working Group on Indicators and Terminology Relating to Disaster Risk Reduction*; A/71/644; United Nations: New York, NY, USA, 2016. Available online: https://www.undrr.org/publication/report-open-ended-intergovernmental-expert-working-group-indicators-and-terminology (accessed on 15 September 2026).
12. Finney, M.A.; McHugh, C.W.; Grenfell, I.C.; Riley, K.L.; Short, K.C. A simulation of probabilistic wildfire risk components for the continental United States. *Stoch. Environ. Res. Risk Assess.* **2011**, *25*, 973–1000. [CrossRef]
13. Stocks, B.J.; Lynham, T.J.; Lawson, B.D.; Alexander, M.E.; Van Wagner, C.E.; McAlpine, R.S.; Dubé, D.E. The Canadian Forest Fire Danger Rating System: An overview. *For. Chron.* **1989**, *65*, 450–457. [CrossRef]
14. Chuvieco, E.; Aguado, I.; Yebra, M.; Nieto, H.; Salas, J.; Martín, M.P.; Vilar, L.; Martínez, J.; Martín, S.; Ibarra, P.; et al. Development of a framework for fire risk assessment using remote sensing and geographic information system technologies. *Ecol. Model.* **2010**, *221*, 46–58. [CrossRef]
15. Jacome Felix Oom, D.; De Rigo, D.; Pfeiffer, H.; Branco, A.; Ferrari, D.; Grecchi, R.; Artes Vivancos, T.; Durrant, T.; Boca, R.; Maianti, P.; et al. *Pan-European Wildfire Risk Assessment*; EUR 31160 EN; Publications Office of the European Union: Luxembourg, 2022. [CrossRef] [PubMed]
16. Martynyuk, A.A.; Savchenkova, V.A.; Korshunov, N.A.; Kotelnikov, R.V. Methods for the use of the best Russian innovations in forest fire detection and suppression. *J. For. Res.* **2021**, *32*, 2255–2263. [CrossRef]
17. Baranovskiy, N. Deterministic-probabilistic approach to predict lightning-caused forest fires in mounting areas. *Forecasting* **2021**, *3*, 695–715. [CrossRef]
18. Hollis, J.J.; Matthews, S.; Fox-Hughes, P.; Grootemaat, S.; Heemstra, S.; Kenny, B.J.; Sauvage, S. Introduction to the Australian Fire Danger Rating System. *Int. J. Wildland Fire* **2024**, *33*, WF23140. [CrossRef]
19. Lim, C.; Chae, H. Characterizing Human-Caused Wildfire Based on the Fire Weather Index in South Korea. *Fire* **2026**, *9*, 147. [CrossRef]
20. An, M.; Kim, D. Do Standard Ignition Indicators Hold in Densely Settled Landscapes? Forest Edges, Trails and Roads in Human-Caused Wildfires of Gyeonggi-do, Republic of Korea. *Fire* **2026**, *9*, 486. [CrossRef]
21. Korea Forest Service. *Understanding Wildfires 2026 (Question-and-Answer Booklet)*; Korea Forest Service: Daejeon, Republic of Korea, 2026; p. 28. Available online: https://www.forest.go.kr/kfs/images/data/down/sb_3_01.pdf (accessed on 12 September 2026). (In Korean)
22. Cova, T.J.; Drews, F.A.; Siebeneck, L.K.; Musters, A. Protective actions in wildfires: Evacuate or shelter-in-place? *Nat. Hazards Rev.* **2009**, *10*, 151–162. [CrossRef]
23. Gyeonggi Province Forest Environment Research Institute. *2025 Spring Wildfire Prevention Plan for Provincial Forests*; Gyeonggi Province: Osan, Republic of Korea, 2025. Available online: https://forest.gg.go.kr/data/42 (accessed on 11 September 2026). (In Korean)
24. MBC Newsdesk. Uiseong Wildfire Spread at a Record 8.2 km per Hour, "Faster than Running" (Thermal Detection Analysis by the National Center for Forest Satellite Information). 27 March 2025. Available online: https://imnews.imbc.com/replay/2025/nwdesk/article/6700494_36799.html (accessed on 11 September 2026). (In Korean)
25. Central Disaster and Safety Countermeasures Headquarters (Joint Release of Relevant Ministries). Rebuilding Lives Destroyed by Wildfires Together—Damage from the Gyeongbuk, Gyeongnam and Ulsan Wildfires Confirmed at KRW 1.0818 Trillion and Recovery Costs at KRW 1.8809 Trillion (Press Release). 2 May 2025. Available online: https://www.mois.go.kr/frt/bbs/type010/commonSelectBoardArticle.do?bbsId=BBSMSTR_000000000008&nttId=117540 (accessed on 11 September 2026). (In Korean)
26. Greenpeace East Asia Seoul Office; Korea Green Transition Institute; Disaster Victims' Rights Center "Urihamkke". *Final Report of the Damage Survey on the 2025 Yeongnam Megafire: Focusing on Andong, Yeongdeok and Uiseong*. 2026. Available online: https://www.greenpeace.org/korea/report/36753/report-yeongnam-mega-wildfire/ (accessed on 11 September 2026). (In Korean)
27. Seoul Shinmun. Vulnerable Groups Helpless Again in Disaster: Wildfire Claims the Lives of 28 Older Adults (Tally by the Korea Forest Service, Gyeongbuk and Gyeongnam Provinces and Police). 1 April 2025. Available online: https://www.seoul.co.kr/news/newsView.php?id=20250401008004 (accessed on 11 September 2026). (In Korean)
28. MBC. Evacuation Order Issued to All Residents of Andong. 25 March 2025. Available online: https://news.imbc.com/news/2025/society/article/6699569_36718.html (accessed on 11 September 2026). (In Korean)
29. JoongAng Ilbo. "We Lifted the Wheelchairs with All Our Might": The Desperate Evacuation of a Senior Residence Where Three Died. 26 March 2025. Available online: https://www.joongang.co.kr/article/25323688 (accessed on 11 September 2026). (In Korean)

30. Heo, S.; Ahn, S.; Lee, Y.-E.; Jung, S.-C.; Jang, M. Bridging Climate and Socio-Environmental Vulnerability for Wildfire Risk Assessment Using Explainable Machine Learning: Evidence from the 2025 Wildfire in Korea. *Forests* **2026**, *17*, 182. [CrossRef]
31. Ministry of the Interior and Safety. Government to Improve Resident Evacuation Systems for Ultra-Fast Wildfires (Press Release). 16 April 2025 (online), 17 April 2025 (print). Available online: https://www.mois.go.kr/frt/bbs/type010/commonSelectBoardArticle.do?bbsId=BBSMSTR_000000000008&nttId=117125 (accessed on 11 September 2026). (In Korean)
32. Ministry of the Interior and Safety. Follow-Up Review Meeting on the Resident Evacuation System for Ultra-Fast Wildfires (Press Release). 7 May 2025 (Online), 8 May 2025 (Print). Available online: https://www.mois.go.kr/frt/bbs/type010/commonSelectBoardArticle.do?bbsId=BBSMSTR_000000000008&nttId=117555 (accessed on 11 September 2026). (In Korean)
33. Ministry of the Interior and Safety; Ministry of Health and Welfare; Korea Forest Service. *Guideline for Evacuation Planning at Wildfire-Vulnerable Special Care Facilities (Draft)*, January 2026; (In Korean; a practical reference that does not take precedence over statutes).
34. McNamee, M.; Pagnon Eriksson, C.; Wahlqvist, J.; Johansson, N. A methodology for assessing wildfire hazard in Sweden–The first step towards a multi-hazard assessment method. *Int. J. Disaster Risk Reduct.* **2022**, *83*, 103415. [CrossRef]
35. Björck, J.; McNamee, M.; Wahlqvist, J.; Larson, M.; Inamdeen, F. A methodology for assessing multiple hazards applied to Sweden. *Int. J. Disaster Risk Reduct.* **2024**, *114*, 104934. [CrossRef]
36. Heo, S.; Ahn, S. Predicting wildfires triggered by human-caused ignition: A spatial framework integrating AI models. *Ecol. Inform.* **2026**, *94*, 103640. [CrossRef]
37. Ji, H.; Lee, G.; Park, J. Wildfire Susceptibility Mapping for Wildland–Urban Interface Areas: A Case Study of Gangneung City, South Korea. *Forests* **2026**, *17*, 934. [CrossRef]
38. Li, S.; Wu, M.; Ye, J.; Zhao, X.; Duan, S.X.; Xue, M.; Yang, W.; Huang, Z.; Han, B.; He, S.; et al. Fine-Scale Mapping of the Wildland–Urban Interface and Seasonal Wildfire Susceptibility Analysis in the High-Altitude Mountainous Areas of Southwestern China. *Fire* **2026**, *9*, 140. [CrossRef]
39. Dang, S.; Kong, X.; Fang, L.; Yang, J.; Tian, X.; Chen, Z.; Xie, Z.; Chen, J.; Ren, S.; Wang, Q. Wildland-urban interface delineation using self-adaptive thresholding informed by historical wildfire patterns: A case study using very-high-resolution satellite imagery and deep learning algorithm. *Sustain. Cities Soc.* **2026**, *145*, 107469. [CrossRef]
40. Kuligowski, E.D. Evacuation decision-making and behavior in wildfires: Past research, current challenges and a future research agenda. *Fire Saf. J.* **2021**, *120*, 103129. [CrossRef]
41. Kuligowski, E.D.; Zhao, X.; Lovreglio, R.; Xu, N.; Yang, K.; Westbury, A.; Nilsson, D.; Brown, N. Modeling evacuation decisions in the 2019 Kincade fire in California. *Saf. Sci.* **2022**, *146*, 105541. [CrossRef]
42. Zhao, X.; Xu, Y.; Lovreglio, R.; Kuligowski, E.; Nilsson, D.; Cova, T.J.; Wu, A.; Yan, X. Estimating wildfire evacuation decision and departure timing using large-scale GPS data. *Transp. Res. Part D Transp. Environ.* **2022**, *107*, 103277. [CrossRef]
43. Wong, S.D.; Broader, J.C.; Walker, J.L.; Shaheen, S.A. Understanding California wildfire evacuee behavior and joint choice making. *Transportation* **2023**, *50*, 1165–1211. [CrossRef]
44. Wahlqvist, J.; Ronchi, E.; Gwynne, S.M.V.; Kinateder, M.; Rein, G.; Mitchell, H.; Bénichou, N.; Ma, C.; Kimball, A.; Kuligowski, E. The simulation of wildland-urban interface fire evacuation: The WUI-NITY platform. *Saf. Sci.* **2021**, *136*, 105145. [CrossRef]
45. Mitchell, H.; Gwynne, S.; Ronchi, E.; Kalogeropoulos, N.; Rein, G. Integrating wildfire spread and evacuation times to design safe triggers: Application to two rural communities using PERIL model. *Saf. Sci.* **2023**, *157*, 105914. [CrossRef]
46. Kalogeropoulos, N.; Mitchell, H.; Ronchi, E.; Gwynne, S.; Rein, G. Design of stochastic trigger boundaries for rural communities evacuating from a wildfire. *Fire Saf. J.* **2023**, *140*, 103854. [CrossRef]
47. Sun, Y.; Forrister, A.; Kuligowski, E.D.; Lovreglio, R.; Cova, T.J.; Zhao, X. Social vulnerabilities and wildfire evacuations: A case study of the 2019 Kincade fire. *Saf. Sci.* **2024**, *176*, 106557. [CrossRef]
48. Niu, C.; Nair, D.J.; Zhang, T.; Dixit, V.; Murray-Tuite, P. Are wildfire fatalities related to road network characteristics? A preliminary analysis of global wildfire cases. *Int. J. Disaster Risk Reduct.* **2022**, *80*, 103217. [CrossRef]
49. Fong, C.R.; Broderick, C.W.; Moritz, M.A.; Halpern, B.S. Egress thresholds and wildfire fatalities. *Proc. Natl. Acad. Sci. USA* **2026**, *123*, e2535081123. [CrossRef] [PubMed]
50. Nunes, A.N.; Pinto, C.D.; Figueiredo, A.; Lourenço, L. Planning wildfire evacuation in the wildland–urban interfaces of central Portugal. *Fire* **2024**, *7*, 199. [CrossRef]
51. Welfare of Senior Citizens Act, Article 32 (Residential Welfare Facilities for the Elderly) and Article 34 (Medical Welfare Facilities for the Elderly). Korean Law Information Center. (In Korean)
52. Modaresi Rad, A.; Abatzoglou, J.T.; Fleishman, E.; Mockrin, M.H.; Radeloff, V.C.; Pourmohamad, Y.; Cattau, M.; Johnson, J.M.; Higuera, P.; Nauslar, N.J.; et al. Social vulnerability of the people exposed to wildfires in U.S. West Coast states. *Sci. Adv.* **2023**, *9*, eadh4615. [CrossRef] [PubMed]
53. Dhungana, B.; Liu, W. Urban–Rural Exposure to Flood Hazard and Social Vulnerability in the Conterminous United States. *ISPRS Int. J. Geo-Inf.* **2024**, *13*, 339. [CrossRef]

54. Gelabert, P.J.; Jiménez-Ruano, A.; Ochoa, C.; Alcasena, F.; Sjöström, J.; Marrs, C.; Ribeiro, L.M.; Palaiologou, P.; Bentué Martínez, C.; Chuvieco, E.; et al. Assessing human-caused wildfire ignition likelihood across Europe. *Nat. Hazards Earth Syst. Sci.* **2025**, *25*, 4713–4729. [CrossRef]
55. Park, J.; Suh, J.; Baek, M. Climatic and Forest Drivers of Wildfires in South Korea (1980–2024): Trends, Predictions, and the Role of the Wildland–Urban Interface. *Forests* **2025**, *16*, 1476. [CrossRef]
56. Radeloff, V.C.; Hammer, R.B.; Stewart, S.I.; Fried, J.S.; Holcomb, S.S.; McKeefry, J.F. The wildland–urban interface in the United States. *Ecol. Appl.* **2005**, *15*, 799–805. [CrossRef]
57. Radeloff, V.C.; Helmers, D.P.; Kramer, H.A.; Mockrin, M.H.; Alexandre, P.M.; Bar-Massada, A.; Butsic, V.; Hawbaker, T.J.; Martinuzzi, S.; Syphard, A.D.; et al. Rapid growth of the US wildland-urban interface raises wildfire risk. *Proc. Natl. Acad. Sci. USA* **2018**, *115*, 3314–3319. [CrossRef] [PubMed]
58. Fernández-García, V.; Beltrán-Marcos, D.; Calvo, L. Building patterns and fuel features drive wildfire severity in wildland-urban interfaces in Southern Europe. *Landsc. Urban Plan.* **2023**, *231*, 104646. [CrossRef]
59. Dresser, C.; Bedi, N.S.; Schroeder, A.; Sergienko, E.; Balsari, S. Proximity of Wildfires to Inpatient Healthcare Facilities in California, 2001–2023. *GeoHealth* **2026**, *10*, e2025GH001531. [CrossRef] [PubMed]
60. Flores, I.; Ortuño, M.T.; Tirado, G. A goal programming model for early evacuation of vulnerable people and relief distribution during a wildfire. *Saf. Sci.* **2023**, *164*, 106117. [CrossRef]
61. Knapp, E.E.; Valachovic, Y.S.; Quarles, S.L.; Johnson, N.G. Housing arrangement and vegetation factors associated with single-family home survival in the 2018 Camp Fire, California. *Fire Ecol.* **2021**, *17*, 25. [CrossRef]
62. Cosgun, U.; Coşkun, M.; Toprak, F.; Yıldız, D.; Coşkun, S.; Taşoğlu, E.; Öztürk, A. Visibility Evaluation and Suitability Analysis of Fire Lookout Towers in Mediterranean Region, Southwest Anatolia/Türkiye. *Fire* **2023**, *6*, 305. [CrossRef]
63. Heyns, A.; du Plessis, W.; Kosch, M.; Hough, G. Optimisation of tower site locations for camera-based wildfire detection systems. *Int. J. Wildland Fire* **2019**, *28*, 651–665. [CrossRef]
64. Heyns, A.M.; du Plessis, W.; Curtin, K.M.; Kosch, M.; Hough, G. Analysis and exploitation of landforms for improved optimisation of camera-based wildfire detection systems. *Fire Technol.* **2021**, *57*, 2269–2303. [CrossRef]
65. Wang, Y.; Gao, G.; Wang, A.; Wang, A.; Liu, J. GIS-Based Wildfire Susceptibility Mapping and Firefighting Access Route Planning in Primeval Forests. *Fire* **2026**, *9*, 343. [CrossRef]
66. Ma, F.; Lee, J.Y. Analyzing wildfire evacuation dynamics with agent-based modeling in damaged road networks. *Saf. Sci.* **2025**, *187*, 106835. [CrossRef]
67. OECD; European Commission Joint Research Centre. *Handbook on Constructing Composite Indicators: Methodology and User Guide*; OECD Publishing: Paris, France, 2008. [CrossRef]
68. Mihajlovski, B.; Zhiyanski, M. Global Forest Fire Assessment Methods: A Comparative Analysis of Hazard, Susceptibility, and Vulnerability Approaches in Different Landscapes. *Fire* **2025**, *8*, 380. [CrossRef]
69. Clifford, P.; Richardson, S.; Hémon, D. Assessing the significance of the correlation between two spatial processes. *Biometrics* **1989**, *45*, 123–134. [CrossRef]
70. Dutilleul, P.; Clifford, P.; Richardson, S.; Hémon, D. Modifying the t test for assessing the correlation between two spatial processes. *Biometrics* **1993**, *49*, 305–314. [CrossRef]
71. Ministry of the Interior and Safety. *Standards and Operating Regulations for Disaster Text Message Broadcasting*; (MOIS Established Rule No. 361, in force 4 February 2026); Annex 2: Standard Messages for Mobile Disaster Alerts; Korean Law Information Center: Sejong-si, Republic of Korea. (In Korean)
72. Grajdura, S.; Qian, X.; Niemeier, D. Awareness, departure, and preparation time in no-notice wildfire evacuations. *Saf. Sci.* **2021**, *139*, 105258. [CrossRef]
73. Cuesta, A.; Balboa, A.; Kuligowski, E.; Alvear, D. Evacuation decisions in the 2023 Tenerife fire: Insights from a comparison with the 2019 Kincade fire. *Fire Saf. J.* **2026**, *162*, 104777. [CrossRef]
74. Siam, M.R.K.; Staes, B.M.; Lindell, M.K.; Wang, H. Lessons learned from the 2018 Attica wildfire: Households' expectations of evacuation logistics and evacuation time estimate components. *Fire Technol.* **2025**, *61*, 795–827. [CrossRef]
75. Teague, B.; McLeod, R.; Pascoe, S. *2009 Victorian Bushfires Royal Commission: Interim Report*; (Recommendation 8.5); Parliament of Victoria: Melbourne, Australia, 2009.
76. Country Fire Authority (CFA). Neighbourhood Safer Places–Bushfire Place of Last Resort. Available online: https://www.cfa.vic.gov.au/plan-prepare/your-local-area-info-and-advice/neighbourhood-safer-places (accessed on 11 September 2026).
77. Parliament of Victoria. *Country Fire Authority Act 1958 (Vic), ss. 50F, 50G, 50J*; Parliament of Victoria: Melbourne, Australia.
78. Autoridade Nacional de Emergência e Proteção Civil (ANEPC). Programa Aldeia Segura, Pessoas Seguras (Resolução do Conselho de Ministros n.º 157-A/2017, de 27 de outubro). Available online: https://prociv.gov.pt/pt/prevencao-e-preparacao/programas-e-projetos/aldeia-segura-pessoas-seguras/ (accessed on 11 September 2026).

79. República Portuguesa. Programa Aldeia e Pessoas Seguras (Comunicado, 14 June 2018). Available online: https://www.portugal.gov.pt/pt/gc21/comunicacao/comunicado?i=programa-aldeia-e-pessoas-seguras (accessed on 11 September 2026).
80. Lim, C.; Chae, H. Application of the Canadian Fire Weather Index for Forest Fire Danger Assessment in South Korea. *Forests* **2025**, *16*, 1058. [CrossRef]

Disclaimer/Publisher's Note: The statements, opinions and data contained in all publications are solely those of the individual author(s) and contributor(s) and not of MDPI and/or the editor(s). MDPI and/or the editor(s) disclaim responsibility for any injury to people or property resulting from any ideas, methods, instructions or products referred to in the content.